iScience

CellPress
OPEN ACCESS

Article

MYC-mediated silencing of miR-181a-5p promotes pathogenic Th17 responses by modulating AKT3-FOXO3 signaling

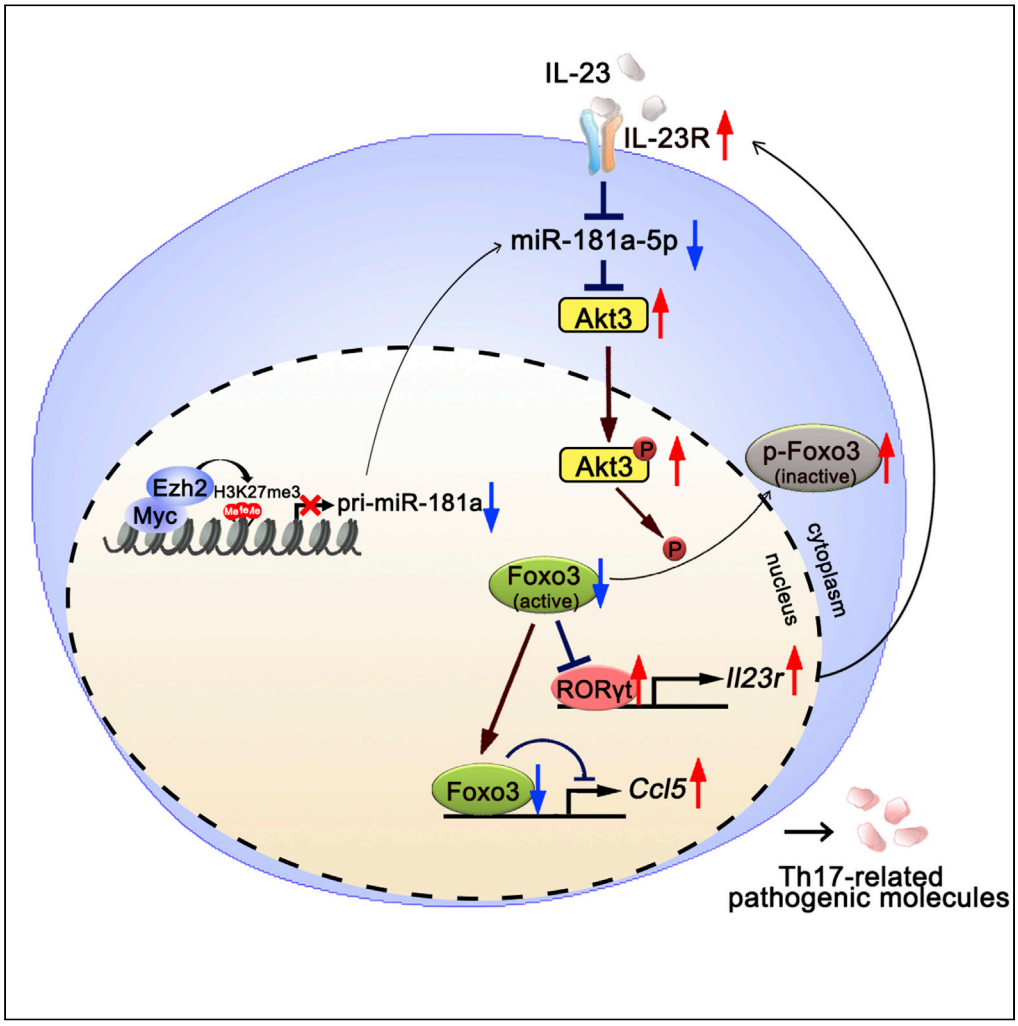

Sisi Chen, Binyun Ma, Xue Li, ..., Ruihua Wei, Xiaorong Li, Hong Nian

nianhong@126.com (H.N.)
xiaorli@163.com (X.L.)

Highlights

MiR-181a-5p inhibits Th17 cell pathogenicity and EAU development

AKT3 is a direct target of miR-181a-5p in pathogenic Th17 cells

MiR-181a-5p represses Th17 cell responses by regulating AKT3-FOXO3 signaling

MYC acts as an upstream suppressor of miR-181a-5p in pathogenic Th17 cells

Chen et al., iScience *25*, 105176
October 21, 2022
https://doi.org/10.1016/j.isci.2022.105176

iScience

CellPress
OPEN ACCESS

Article

MYC-mediated silencing of miR-181a-5p promotes pathogenic Th17 responses by modulating AKT3-FOXO3 signaling

Sisi Chen,[1,3] Binyun Ma,[2,3] Xue Li,[1,3] Kailang Zhang,[1] Yankai Wei,[1] Bei Du,[1] Xun Liu,[1] Ruihua Wei,[1] Xiaorong Li,[1,*] and Hong Nian[1,4,*]

SUMMARY

Pathogenic Th17 cells drive autoimmune pathology, but the molecular mechanisms underlying Th17 pathogenicity remain poorly understood. Here, we have shown that miR-181a-5p was significantly decreased in pathogenic Th17 cells, and it negatively regulated pathogenic Th17 cell responses *in vitro* and *in vivo*. Th17 cells overexpressing miR-181a-5p exhibited impaired ability to induce pathogenesis in an adoptive transfer model of experimental autoimmune uveitis (EAU). Mechanistically, miR-181a-5p directly targeted AKT3, diminishing AKT3-mediated phosphorylation of FOXO3, and thereby activating FOXO3, a transcriptional repressor of pathogenic Th17 cell program. Supporting this, decreasing miR-181a-5p and up-regulated *AKT3* expression were found in uveitis patients. Furthermore, intravitreal administration of miR-181a-5p mimics in mice effectively attenuated clinical and pathological signs of established EAU. Collectively, our results reveal a previously unappreciated T cell-intrinsic role of miR-181a-5p in restraining autoimmunity and may provide a potential therapeutic target for uveitis treatment.

INTRODUCTION

Th17 cells drive the pathogenesis of various autoimmune disorders, including uveitis and its animal model, experimental autoimmune uveitis (EAU) (Amadi-Obi et al., 2007; Chong et al., 2020; Zhong et al., 2021). The integrated cytokine signaling induced by TGF-β, IL-1β, IL-6, and IL-23 promote the expression of the lineage-defining transcription factor RORγt and subsequent Th17 cell program (Lee et al., 2012). Accumulating evidences demonstrate that Th17 cells induced by TGF-β and IL-6 secrete immunoregulatory cytokine IL-10 and are largely nonpathogenic (McGeachy et al., 2007), and Th17 cells require IL-23 for their pathogenic effector functions (Ghoreschi et al., 2010; Lee et al., 2012). Compared to nonpathogenic Th17 cells, pathogenic Th17 cells express high levels of *Il23r*, *Il1r1*, *Csf2* and *Ccl5* (Hu et al., 2017; Lee et al., 2012). Yet, despite extensive studies conducted both *in vivo* and *in vitro*, the molecular mechanisms underlying pathogenic Th17 cell function are insufficiently understood.

miRNAs (miRs), a class of small non-coding RNAs that negatively regulate gene expression at the post-transcriptional level, have been reported to affect autoimmunity (Mehta and Baltimore, 2016; Singh et al., 2014). Deficiency of Dicer leads to the development of autoimmune diseases (O'Connell et al., 2010). Moreover, published works have verified that certain miRs play a pivotal role in pathogenic Th17 cells. Knocking out or knocking down miR-183C or miR-301a results in decreased pathogenic Th17 cell responses *in vitro* and *in vivo* (Ichiyama et al., 2016; Mycko et al., 2012). However, the roles of miRs in regulation of pathogenic Th17 cells induced by IL-23 are still largely unknown.

miR-181a has been implicated in immune responses (Kim et al., 2021). miR-181a-5p is the main mature form of miR-181a precursor (Griffiths-Jones et al., 2008). It restrains M1 macrophage polarization (Bi et al., 2016), promotes $CD4^+$ T cell differentiation toward the Treg and Th2 subsets and inhibits Th1 differentiation (Liu et al., 2019; Sang et al., 2015). Recently, it has been linked to Th17 cell differentiation (He et al., 2022; Sang et al., 2015). However, the cell-intrinsic function of miR-181a-5p in the regulation of pathogenic Th17 cells remains unclear.

[1]Tianjin Key Laboratory of Retinal Functions and Diseases, Tianjin Branch of National Clinical Research Center for Ocular Disease, Eye Institute and School of Optometry, Tianjin Medical University Eye Hospital, Tianjin 300384, China

[2]Department of Medicine/Hematology, Keck School of Medicine of the University of Southern California, Los Angeles, CA 90033, USA

[3]These authors contributed equally

[4]Lead contact

*Correspondence: nianhong@126.com (H.N.), xiaorli@163.com (X.L.)

https://doi.org/10.1016/j.isci.2022.105176

In this study, we showed that pathogenic Th17 cell function was regulated by miR-181a-5p. Furthermore, miR-181a-5p targeted AKT3 to control pathogenic Th17 cell responses via modulating AKT3-regulated FOXO3-dependent gene expression program. Th17 cells overexpressing miR-181a-5p displayed impaired ability to induce EAU. Notably, local administration of miR-181a-5p effectively ameliorated clinical and pathological signs of established EAU. Collectively, our findings reveal a previously unrecognized role of miR-181a-5p in autoimmunity, which may have clinical implications.

RESULTS

miR-181a-5p down-regulated in antigen-specific Th17 cells negatively regulates Th17 responses

To uncover potential EAU-suppressor miRs that are significantly down-regulated in EAU, we performed miRNA microarray analysis in EAU $CD4^+$ T cells and naive $CD4^+$ T cells. As shown in Figure 1A, we found that 14 miRs were down-regulated at least 2-fold in EAU $CD4^+$ T cells compared to controls. Among these, miR-181a-5p was the most down-regulated miR, which was further confirmed by real-time qRT-PCR (Figures 1B and S1). Given that it was also significantly decreased in uveitis patients by excavating miRNA microarray data in GSE145191 (Figure 1C), we focused on miR-181a-5p in the subsequent studies. We examined the expression of miR-181a-5p in several Th subsets and found that it was significantly decreased in Th17 cells compared with that in Th1 and Th0 cells (Figure 1D). Further analysis revealed that IL-23 inhibited miR-181a-5p expression in a dose-dependent way (Figure 1E). We next determined the relevance between miR-181a-5p level and the disease process of EAU, and found that miR-181a-5p expression was significantly reduced in Th17 cells during the course of EAU and was closely correlated with disease severity (Figure 1F).

To examine the role of miR-181a-5p in IRBP-Th17 responses, $CD4^+$ T cells from EAU mice transfected with miR-181a-5p mimics, inhibitor or their corresponding controls were co-cultured with antigen-presenting cells (APCs) and immunizing antigen ($IRBP_{1\text{-}20}$) or irrelevant antigen ($OVA_{323\text{-}339}$) under Th17-polarizing conditions. As shown in Figure 1G, T cells overexpressing miR-181a-5p exhibited significantly reduced IL-17 production, when T cells were restimulated with IL-23 and APCs in the presence of $IRBP_{1\text{-}20}$, but not in the presence of $OVA_{323\text{-}339}$. Consistent with the change of IL-17 secretion, Th17 cell percentages (Figure 1H) and the expression of pathogenic Th17 signature genes, such as *Il17*, *Csf2*, *Ccl5*, *Il23r*, and *Il1r1* (Figure 1I), were also significantly decreased in miR-181a-5p mimics-transfected cells relative to control group. In addition, knockdown of miR-181a-5p dramatically promoted the production of IL-17 (Figure 1J) and the expression of *Il17*, *Csf2*, *Ccl5*, *Il23r*, and *Il1r1* mRNA (Figure 1K). These data indicate that miR-181a-5p serves as a negative regulator of pathogenic Th17 responses *in vitro*.

Overexpression of miR-181a-5p attenuates EAU and pathogenic Th17 responses

To investigate the *in vivo* effect of miR-181a-5p on EAU pathogenesis, we overexpressed miR-181a-5p by intravenous injecting with approximately 5×10^7 transducing units (TU) of lentivirus-miR-181a (LV-181a) into C57BL/6 mice before EAU induction (Du et al., 2009) (Figure 2A). As shown in Figure S2B, administration of LV-181a resulted in a significant increase of miR-181a-5p in several organs. After immunization, severe vasculitis, multiple chorioretinal lesions and papilledema were observed in LV-Ctrl-infected mice, whereas LV-181a-infected mice exhibited significantly attenuated EAU (Figure 2B). Histological analysis showed that inflammatory infiltration and retinal damage were also dramatically reduced in LV-181a-infected mice compared with the control group (Figure 2C).

We then sought to determine whether the attenuated EAU induced by miR-181a-5p was because of the altered Th17 responses. To this end, $CD4^+$ T cells isolated from different groups were restimulated with $IRBP_{1\text{-}20}$ and APCs under Th17 cell polarizing conditions, and we found that relative to the control group, IRBP-specific Th17 responses from LV-181a-infected mice were reduced as shown by significantly reduced percentages of Th17 cells and greatly decreased IL-17 production (Figures 2D and 2E). Further analysis revealed that signature genes of pathogenic Th17 cells, including *Il17*, *Rorc*, *Csf2*, *Il23r*, *Ccl5*, and *Tbx21*, were also significantly down-regulated (Figure 2F), whereas genes related to Treg cell subsets, such as *Il10*, *Tgfb*, *Ahr*, and *Foxp3*, were markedly up-regulated in T cells from LV-181a-infected mice (Figure 2G). In line with the change of Treg-related gene expression, the proportion of Treg cells in the T cells from LV-181a-infected mice was increased when compared to the control group (Figure 2H). Moreover, miR-181a-5p treatment significantly decreased the expression of proinflammatory cytokines including *Il1b*, *Il23*, *Il6*,

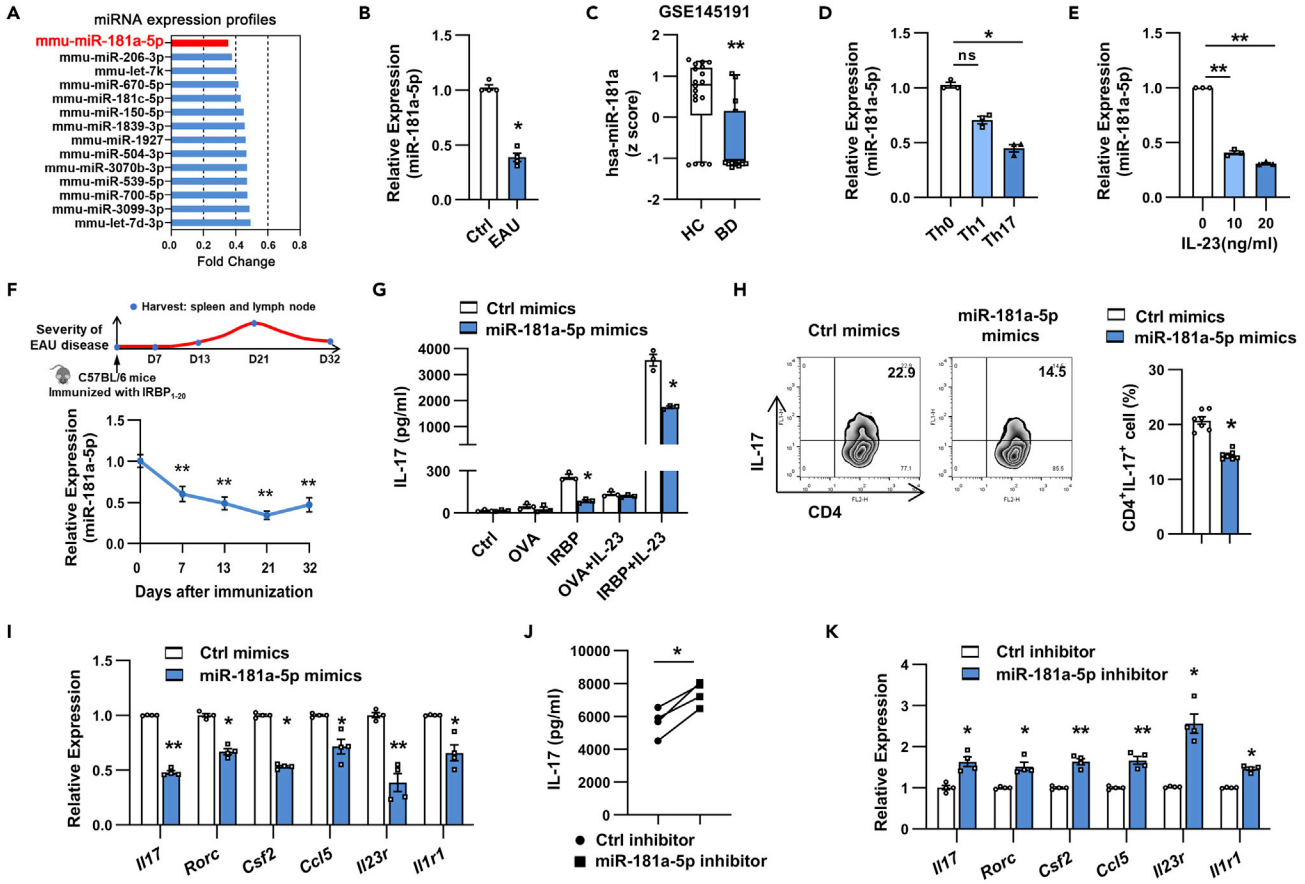

Figure 1. miR-181a-5p down-regulated in IRBP-specific Th17 cells suppressed Th17 response *in vitro*

(A) Microarray-based bar graphs showing the down-regulated miRs in $CD4^+$ T cells isolated from EAU mice relative to those from naive mice. $CD4^+$ T cells from 6 mice per group were pooled for microarray analysis.

(B) Real-time qRT-PCR analysis of miR-181a-5p expression in $CD4^+$ T cells from naive (Ctrl) and EAU mice (n = 4 per group).

(C) Down-regulated miR-181a-5p expression was shown in patients with Behçet's disease (BD). The *Z* score transformed values of the microarray gene expression dataset GSE145191 (16 patients with BD and 18 healthy controls).

(D and E) $CD4^+$ T cells were isolated from EAU mice and co-cultured with APCs and $IRBP_{1\text{-}20}$ peptide under indicated conditions for 48 h. Real-time qRT-PCR analysis of miR-181a-5p expression (n = 3 per group).

(F) Schematic diagram of induction and progression of actively induced EAU is shown above. Kinetic analysis of miR-181a-5p expression in IRBP-specific Th17 cells during the course of EAU (n = 5 per group).

(G) ELISA analysis of IL-17 production in $CD4^+$ T cells transfected with miR-181a-5p mimics and restimulated with the indicated antigens and IL-23 (n = 3 per group).

(H–K) $CD4^+$ T cells were transfected with indicated oligonucleotides (300 nM) and stimulated with $IRBP_{1\text{-}20}$ in the presence of irradiated APCs under Th17 polarizing conditions. (H) Flow cytometric analysis of the percentages of the $CD4^+IL\text{-}17^+$ cells (n = 3 per group). (I, K) Real-time qRT-PCR analysis of Th17-related gene expression (n = 4 per group). (J) ELISA analysis of IL-17 secretion in the culture supernatants (n = 4 per group). Data are presented as mean ± SEM of at least three independent experiments. In the statistical analysis, Mann-Whitney U test (B), Kruskal-Wallis test (D), One-way ANOVA (E-F), and Student's t test (G-K) were used with significance defined as *p<0.05, **p<0.01. See also Figure S1.

and *Il12* (Figure 2I). Collectively, these findings suggest a critical role for miR-181a-5p in suppressing pathogenic Th17 cells and EAU.

miR-181a-5p reduces the pathogenicity of Th17 cells

To assess $CD4^+$ T cell-intrinsic function of miR-181a-5p, we utilized the adoptive transfer model of EAU (Nian et al., 2012). $CD4^+$ T cells isolated from $IRBP_{1\text{-}20}$-immunized C57BL/6 mice were transfected with Ctrl or miR-181a-5p mimics and restimulated with $IRBP_{1\text{-}20}$ in the presence of APCs under Th17-polarizing conditions. Two days later, activated Th17 cells were adoptively transferred into naive C57BL/6 mice which were monitored for EAU score by fundus examination (Figure 3A). As shown in Figure 3B, the mice that received Th17 cells transfected with miR-181a-5p mimics developed significantly attenuated EAU

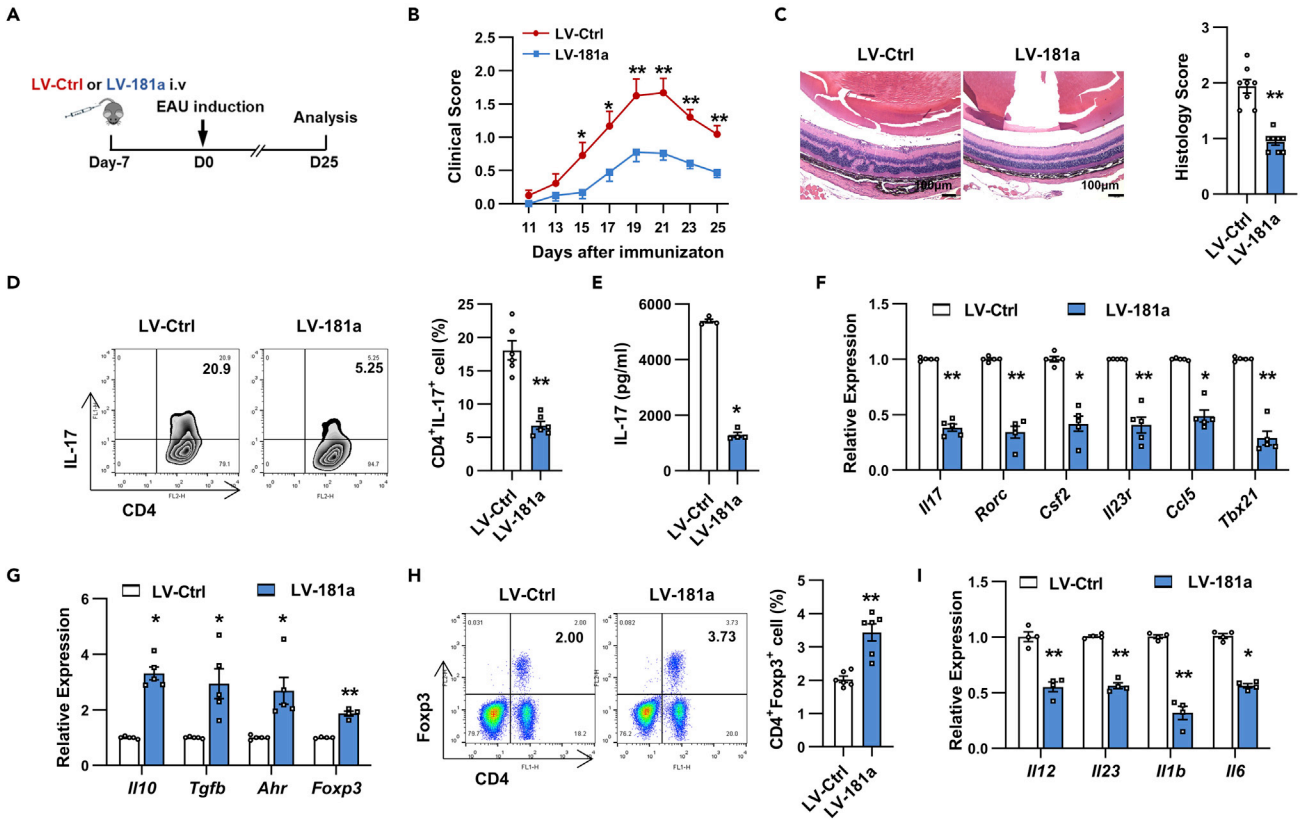

Figure 2. miR-181a-5p attenuated EAU development

(A) Schematic illustration of the experimental approach to study the role of miR-181a-5p in EAU.

(B and C) Clinical scores (B) and histopathological analysis (C) of EAU mice infected with LV-Ctrl or LV-181a (n = 8 mice per group). Scale bars, 100 μm.

(D and E) $CD4^+$ T cells from lentivirus-infected EAU mice were stimulated with APCs and $IRBP_{1\text{-}20}$ under Th17 polarization. (D) Flow cytometric analysis of the percentages of the $CD4^+IL\text{-}17^+$ cells (n = 6 per group). (E) ELISA analysis of IL-17 secretion in the culture supernatants (n = 4 per group).

(F and G) Real-time qRT-PCR analysis of Th17 (F) and Treg (G) signature genes in $CD4^+$ T cells (n = 4 per group).

(H) Flow cytometric analysis of the percentages of the $CD4^+FOXP3^+$ cells (n = 6 per group).

(I) Real-time qRT-PCR analysis of Th17 cell-polarizing cytokines expression in the spleen (n = 4 per group). Data are presented as mean ± SEM of at least three independent experiments. In the statistical analysis, two-way ANOVA (B) and Student's t test (C-I) were used with significance defined as *p<0.05, **p<0.01. See also Figures S2 and S3.

compared with those that received Ctrl mimics-transfected Th17 cells. This trend was also seen at the level of histopathology. The inflammatory infiltration and retinal damage were significantly reduced in mice receiving Th17 cells overexpressing miR-181a-5p relative to the control group (Figure 3C). In addition, the secretion of IL-17 and IFN-γ (Figures 3D and 3E), as well as the relative expression of *Il17* and *Ifng* mRNA (Figure 3F), were significantly decreased in T cells from the mice that received miR-181a-5p mimics-transfected Th17 cells. Further analysis revealed that the expression of *Foxp3* and *Ahr* mRNA, as well as the percentage of Treg cells in the T cells from mice receiving Th17 cells overexpressing miR-181a-5p were increased when compared to the control group (Figures 3F and 3G). miR-181a-5p overexpression in IRBP-specific Th17 cells leads to a significantly less pathogenic EAU phenotype, strongly confirming the T cell-intrinsic role of miR-181a-5p in pathogenic Th17 function.

AKT3 partially mediates decreased pathogenic Th17 responses induced by miR-181a-5p

To understand how miR-181a-5p regulates pathogenic Th17 cell function, we sought to identify the potential miR-181a-5p targets using TarBase, Pictar, StarBase, and Targetscan databases (Figure 4A). Among the predicted targets, *Akt3* attracted our attention due to its role in regulating $CD4^+$ T cell function (DuBois et al., 2019). *Akt3* mRNA has a highly conserved miR-181a-5p binding site within its 3'UTR among vertebrates (Figure 4B). To determine whether *Akt3* is a direct target of miR-181a-5p, luciferase reporter constructs were generated with wildtype (WT) or mutant (mut) *Akt3* 3'UTR. As shown in Figure 4C, luciferase

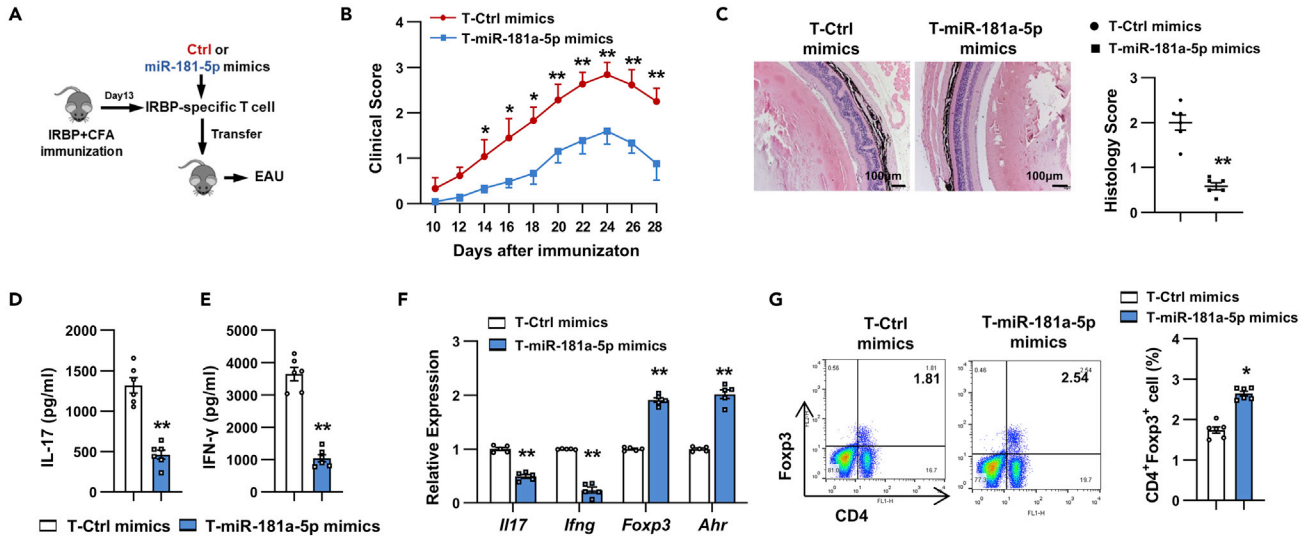

Figure 3. miR-181a-5p overexpression in Th17 cells ameliorates EAU

(A) Schematic of EAU induced by adoptive transfer.

(B and C) Clinical scores (B) and histopathological analysis (C) of EAU (n = 6 per group) in naive C57BL/6 mice adoptively transferred with Ctrl (T-Ctrl mimics) or miR-181a-5p mimics (T-miR-181a-5p mimics)-transfected Th17 cells. Scale bars, 100 μm.

(D and E) $CD4^+$ T cells were isolated from adoptive EAU mice and stimulated with $IRBP_{1\text{-}20}$ in the presence of APCs. ELISA analysis of IL-17 (D) and IFN-γ (E) secretion in the culture supernatants (n = 6 per group).

(F) Real-time qRT-PCR analysis of Th1, Th17, and Treg-related gene expression in $CD4^+$ T cells (n = 5 per group).

(G) Flow cytometric analysis of the percentages of $CD4^+$ $FOXP3^+$ cells (n = 6 per group). Data are presented as mean ± SEM of at least three independent experiments. In the statistical analysis, two-way ANOVA (B) and Student's t test (C–G) were used with significance defined as *p<0.05, **p<0.01.

activity was suppressed by miR-181a-5p mimics in HEK293T cells transfected with *Akt3*-WT 3′UTR but not those transfected with *Akt3*-mut 3′UTR. In addition, real-time qRT-PCR and western blot analysis revealed that AKT3 expression was decreased in miR-181a-5p overexpressing Th17 cells (Figures 4D and 4E), but was increased after miR-181a-5p inhibitor transfection (Figure 4F). Consistent with *in vitro* results, T cells from LV-181a-infected EAU mice also displayed a significantly decreased AKT3 expression (Figure 4G). Further analysis revealed that *Akt3* expression showed a negative correlation with miR-181a-5p expression in Th17 cells during EAU (Figures 4H and 4I). Together, these data indicate that AKT3 is a functional target of miR-181a-5p.

To test whether AKT3 is functionally important for miR-181a-5p-mediated reduced Th17 responses, $CD4^+$ T cells from EAU or mouse T-cell lymphoma cell line EL4 T cells were transfected with siRNA specific for *Akt3* or control siRNA and cultured in Th17 polarizing conditions. As shown in Figure 4J, AKT3 was indeed knockdown by *Akt3* siRNA with a reduction of IL-17 secretion (Figure 4K) and decreased expression of *Il17*, *Rorc*, *Il23r*, *Il1r1*, *Ccl5* and *Tbx21* mRNA (Figure 4L). Similarly, the expression of *Il17*, *Rorc*, *Csf2*, and *Il23r* was also repressed in si*Akt3*-transfected EL4 T cells compared with the control group (Figure 4M). Besides, inhibiting AKT3 activity partially counteracted increased IL-17 production, *Il23r* and *Ccl5* expression induced by miR-181a-5p inhibitor (Figures 4N and 4O). These results suggest that AKT3 may partially mediate the inhibitory effect of miR-181a-5p on pathogenic Th17 cells.

miR-181a-5p overexpression inhibits the AKT3-FOXO3 signaling in Th17 cells

Because FOXO3 is a downstream target of PI3K/AKT3 signaling (Manning and Toker, 2017), we next examined whether miR-181a-5p affects the AKT3/FOXO3 signaling. Overexpression of miR-181a-5p in Th17 cells substantially inhibited AKT3/FOXO3 signaling as indicated by significantly decreased phosphorylation of AKT3 and FOXO3 (Figure 5A). Similar to the *in vitro* results, the phosphorylation levels of AKT3 and FOXO3 in $CD4^+$ T cells from LV-181a-infected EAU mice were also dramatically decreased as compared with control mice (Figure 5B). Given that the phosphorylation of FOXO proteins by AKT could trigger their relocation from the nucleus to the cytosol and therefore inactivate their transcription factor activity (Manning and Toker, 2017), we investigated the effect of miR-181a-5p on the nuclear localization of FOXO3 using an immunofluorescence assay. We found that FOXO3 protein primarily localized to the cytoplasm of EL4

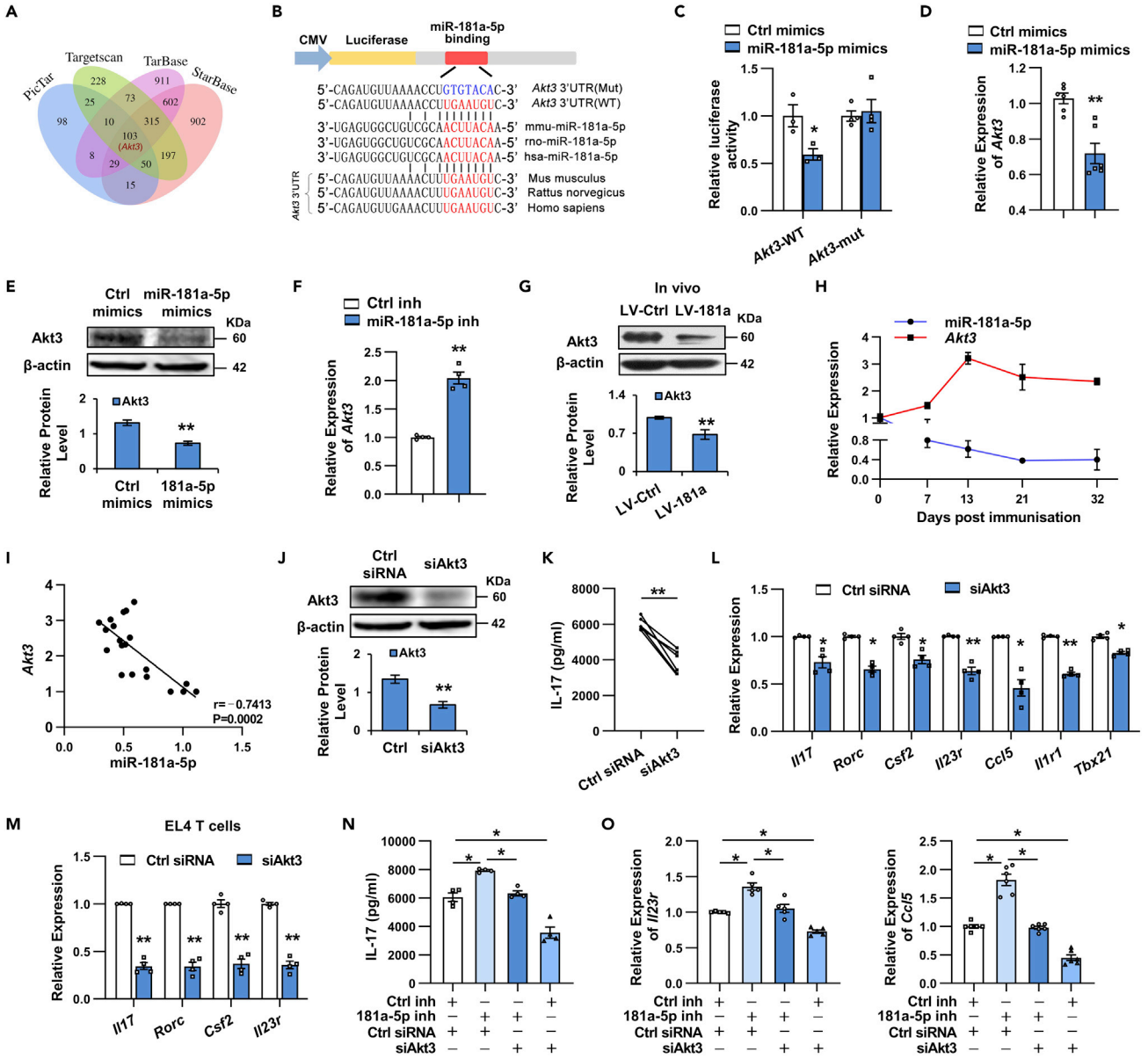

Figure 4. miR-181a-5p regulates pathogenic Th17 responses via suppression of AKT3 expression

(A) Venn diagram analysis of putative miR-181a-5p target genes as predicted by TargetScan, PicTar, TarBase, and StarBase databases.

(B) Sequence alignment between miR-181-5p and its potential binding sites (in red letters) in the *Akt3* 3′UTR among multiple species. The mutation of the miR-181a-5p target sites (in blue letters) is shown above.

(C) Luciferase activity analysis of reporter carrying the wild-type (WT) (n = 3 per group) or mutant (Mut) (n = 4 per group) *Akt3* 3′UTR co-transfected into HEK293T with Ctrl mimics or miR-181a-5p mimics. The relative luciferase activity was calculated as the ratio of Firefly luciferase activity to Renilla luciferase activity.

(D–F) Real-time qRT-PCR (n = 4 per group) and western blot analysis (n = 3 per group) of AKT3 expression in Th17 cells transfected with miR-181a-5p mimics, inhibitor, or their corresponding control.

(G) Western blot analysis of AKT3 expression in $CD4^+$ T cells isolated from the LV-Ctrl or LV-181a-infected EAU mice (n = 4 per group).

(H) The kinetics expression changes of miR-181a-5p and *Akt3* in Th17 cells at various stages of EAU (n = 5 per group).

(I) The correlation between miR-181a-5p expression and *Akt3* levels in Th17 cells during EAU development. p value was calculated by the Pearson correlation test, which was performed on the data of miR-181a-5p and *Akt3* expression in Th17 cells at various stages of EAU (n = 20).

(J–L and N–O) EAU $CD4^+$ T cells were transfected with indicated oligonucleotides under Th17-polarizing conditions. (J) Western blot analysis of AKT3 expression (n = 3 per group). (K, N) ELISA analysis of IL-17 secretion in the culture supernatants (n = 4–6 per group). (L, O) Real-time qRT-PCR analysis of Th17 signature genes (n = 4–6 per group).

Figure 4. *Continued*

(M) Real-time qRT-PCR analysis of Th17 signature genes in EL4 T cells (n = 4 per group). Data are presented as mean ± SEM of at least three independent experiments. In the statistical analysis, Student's t test (C–M) and One-way ANOVA (N and O) were used with significance defined as *p<0.05, **p<0.01. See also Table S3 for the potential targets of miR-181a-5p predicted with miRNA target databases.

T cells and miR-181a-5p overexpression induced FOXO3 nuclear translocation (Figure 5C), suggesting that miR-181a-5p may suppress pathogenic Th17 cell function by activating FOXO3 nuclear translocation.

IL-23R is closely involved in the pathogenicity of Th17 cells (Wu et al., 2013), and RORγt is necessary for IL-23R expression in Th17 cells. We previously reported that FOXO3 suppressed *Il23r* expression, and there was a potential FOXO3 binding site close to the RORγt binding region on the *Il23r* promoter locus (Wei et al., 2019). This led us to hypothesize that FOXO3 might regulate IL-23R expression via affecting RORγt function. To confirm this, we constructed a luciferase reporter containing *Il23r* promoter region to analyze the transcriptional activity of IL-23R. As shown in Figure 5D, FOXO3 efficiently inhibited RORγt induced *Il23r* luciferase activity in HEK293 T cells in a dose-dependent manner, whereas FOXO3 alone did not significantly affect *Il23r* luciferase activity. These data suggest that FOXO3 might negatively regulate IL-23R expression via interference with RORγt activity in Th17 cells.

Ccl5, one of the key pathogenic Th17 cell signature genes (Hu et al., 2017; Lee et al., 2012), plays an important role in the pathogenesis of uveitis (Niu et al., 2019). Here, we observed that FOXO3 significantly suppressed the expression of *Ccl5* in Th17 cells (Figure 5E), and bioinformatic analysis with JASPER (http://jaspar.genereg.net/) revealed the presence of putative FOXO3 binding sites in *Ccl5* promoter region. These suggest that FOXO3 might negatively regulate *Ccl5* transcription via binding its promoter region. To test this, a luciferase reporter containing *Ccl5* promoter region was constructed to analyze the direct role of FOXO3 on *Ccl5* promoter activity. As shown in Figure 5F, FOXO3 dramatically reduced the levels of *Ccl5* promoter activity in a dose-dependent manner, as measured by luciferase activity, suggesting that binding of FOXO3 to the promoter region of *Ccl5* is critical for its transcriptional repression.

Together, these data strongly indicate that dramatic Th17 cell defects associated with miR-181a-5p overexpression are at least in part caused by faulty AKT3-FOXO3 signaling.

MYC and EZH2 inhibit miR-181a-5p expression via histone H3K27 trimethylation in pathogenic Th17 cells

Epigenetic modifications, such as trimethylation of histone 3 lysine 27 (H3K27me3), are key mediators of miRNAs dysregulation (Baer et al., 2013). Recent studies revealed that MYC recruited EZH2, the histone methyltransferase of the polycomb repressive complex 2 catalyzing H3K27me3, to epigenetically silence tumor suppressor genes (Wang et al., 2014; Zhang et al., 2018). We wondered whether miR-181a-5p downregulation in pathogenic Th17 cells has a similar mechanism. We first examined the expression of *Myc* and *Ezh2* in EAU, and observed that both *Myc* and *Ezh2* were significantly increased in IRBP-specific Th17 cells (Figures 6A and 6B). Using siRNA-mediated knockdown of *Myc* or *Ezh2* in Th17 cells (Figure 6C), we further found that either silencing *Myc* or *Ezh2* robustly increased miR-181a-5p and pri-miR-181a expression (Figures 6D and 6E), suggesting the involvement of both MYC and EZH2 in regulation of miR-181a-5p expression. Moreover, we found a broad overlap of MYC and EZH2 occupancy on the miR-181a promoter (Valencia et al., 2020) in T cell (Figure 6F) by analyzing the ChIP-seq datasets of Cistrome Project (http://cistrome.org/). To explore how MYC and EZH2 repress miR-181a transcription, we constructed a luciferase reporter containing miR-181a promoter region. As presented in Figure 6G, co-transfection of siMyc and siEzh2 induced remarkably increased luciferase activity of miR-181a promoter, as compared with transfection with siMyc and siEzh2 alone. However, overexpression of MYC greatly suppressed the luciferase activity of miR-181a promoter and the addition of siEzh2 abolished that (Figure 6H), indicating that MYC might decrease miR-181a-5p expression by recruiting EZH2 to miR-181a promoter. To confirm MYC and EZH2 mediated methyltransferase activity, we sought to identify H3K27me3 marks on the promoter of miR-181a. As shown in Figure 6I, the enrichment of H3K27me3 marks was noted on the miR-181a promoter region in Th17 cells relative to naive $CD4^+$ T cells by analyzing ChIP-seq dataset (GSE14254). Moreover, treatment of Th17 cells with H3K27me3 inhibitor deazaneplanocin A (DZNep) led to robust re-expression of pri-miR-181a and miR-181a-5p (Figure 6J). Collectively, these results indicate that MYC and EZH2 coordinately suppress miR-181-5p expression through H3K27me3 in pathogenic Th17 cells (Figure 6K).

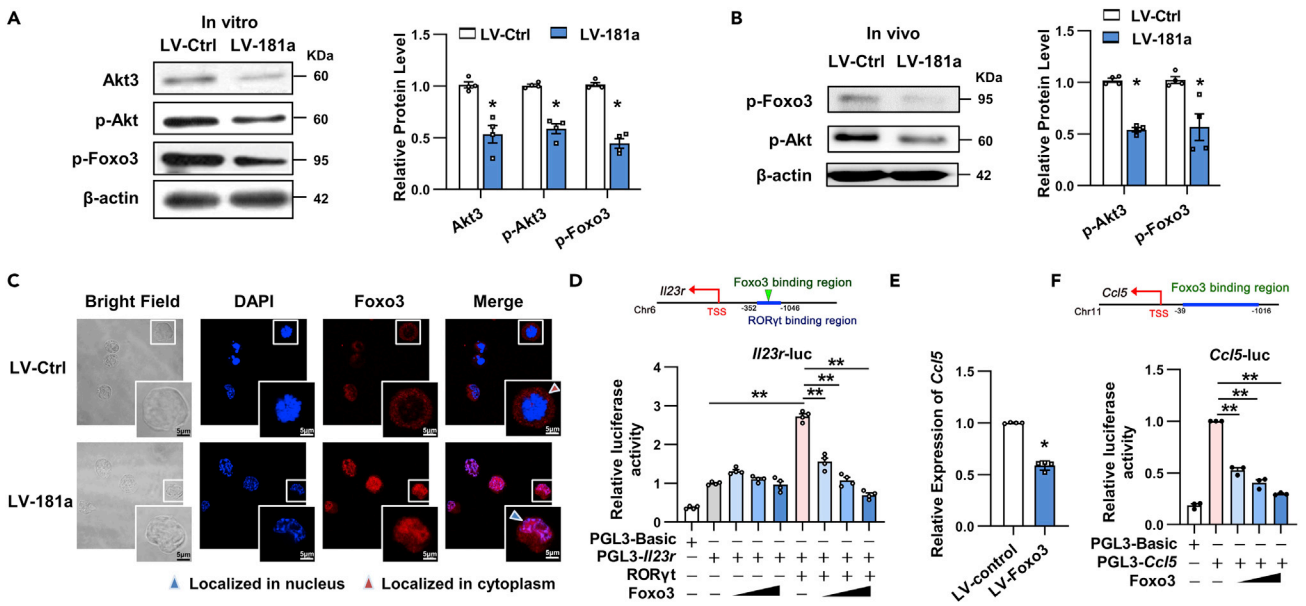

Figure 5. miR-181a-5p modulates the AKT3-FOXO3-IL-23R/CCL5 pathway in Th17 cells

(A and B) Western blot analysis for AKT pathway-associated protein in Th17 cells infected with LV-Ctrl or LV-181a (MOI =50) *in vitro* (A), and in CD4$^+$ T cells isolated from LV-Ctrl or LV-181a-infected EAU mice (B). Statistical analysis data are shown in the right panel (n = 4 per group).

(C) Representative confocal images of FOXO3 (red) immunofluorescent staining in EL4 T cells infected with LV-Ctrl or LV-181a for 48 h through a ×63 oil immersion objective. Scale bars, 5 μm.

(D and F) Luciferase activity analysis of reporter carrying *Il23r* promoter (D) or *Ccl5* promoter (F) co-transfected into HEK293T with the indicated plasmids (n = 3–4 per group).

(E) Real-time qRT-PCR analysis of *Ccl5* expression in Th17 cells infected with FOXO3 lentivirus (LV-FOXO3) or control lentivirus (LV-control) (n = 4 per group).

Data are presented as mean ± SEM of at least three independent experiments. In the statistical analysis, Student's t test (A and B), One-way ANOVA (D, F), and Mann-Whitney U test (E) were used with significance defined as *p<0.05, **p<0.01. See also Figure S4.

Therapeutic benefits of topical administration of miR-181a-5p on EAU

To explore the translational implications of our findings, we examined the therapeutic effect of local miR-181a-5p administration on established EAU. To this, liposomes containing miR-181a-5p mimics or Ctrl mimics were intravitreally injected into EAU mice (Sun et al., 2015) at the early phase of disease (day 11 after EAU induction) (Figure 7A). As shown in Figure 7B, treatment with miR-181a-5p-mimics significantly reduced EAU clinical scores compared to control mice. Consistently, slight inflammatory infiltrates in the retina/vitreous cavity and reduced retinal damage were detected by histopathological analysis in miR-181a-5p mimics treated mice (Figure 7C). These results suggest that miR-181a-5p may be a promising therapeutic target for uveitis treatment.

The MYC/miR-181a-5p/AKT3 pathway in human uveitis

To evaluate the potential clinical relevance of this regulatory pathway in human, we analyzed the publicly available datasets of uveitis patients. miR-181a-5p was down-regulated in the peripheral blood mononuclear cells (PBMCs) of Behçet's disease (BD) patients (Puccetti et al., 2018) and enucleated globes of sympathetic ophthalmia (Kaneko et al., 2012) (Figure 8A). Also, upregulated expression of *AKT3* was observed in PBMCs of patients with BD (Figure 8B), and a positive correlation between the expression of *AKT3* and pathogenic Th17 signature genes (including *IL-17*, *RORC*, *IL-23R*, *GM-CSF* and *CCL5*) was shown in CD4$^+$ T cells from BD patients (Figure 8C). Moreover, *MYC* was up-regulated in the CD4$^+$ T cells of BD patients (Figure 8D). These findings suggest that similar to mouse the potential regulatory pathway of MYC/miR-181a-5p/AKT3 appears to operate in human uveitis.

DISCUSSION

miRs are important for Th17 cell function in autoimmunity. However, limited information is available on the roles of miRs in pathogenic Th17 cell responses. In this study, we revealed a previously unrecognized role of miR-181a-5p in controlling pathogenic Th17 cells. miR-181a-5p was significantly decreased in pathogenic

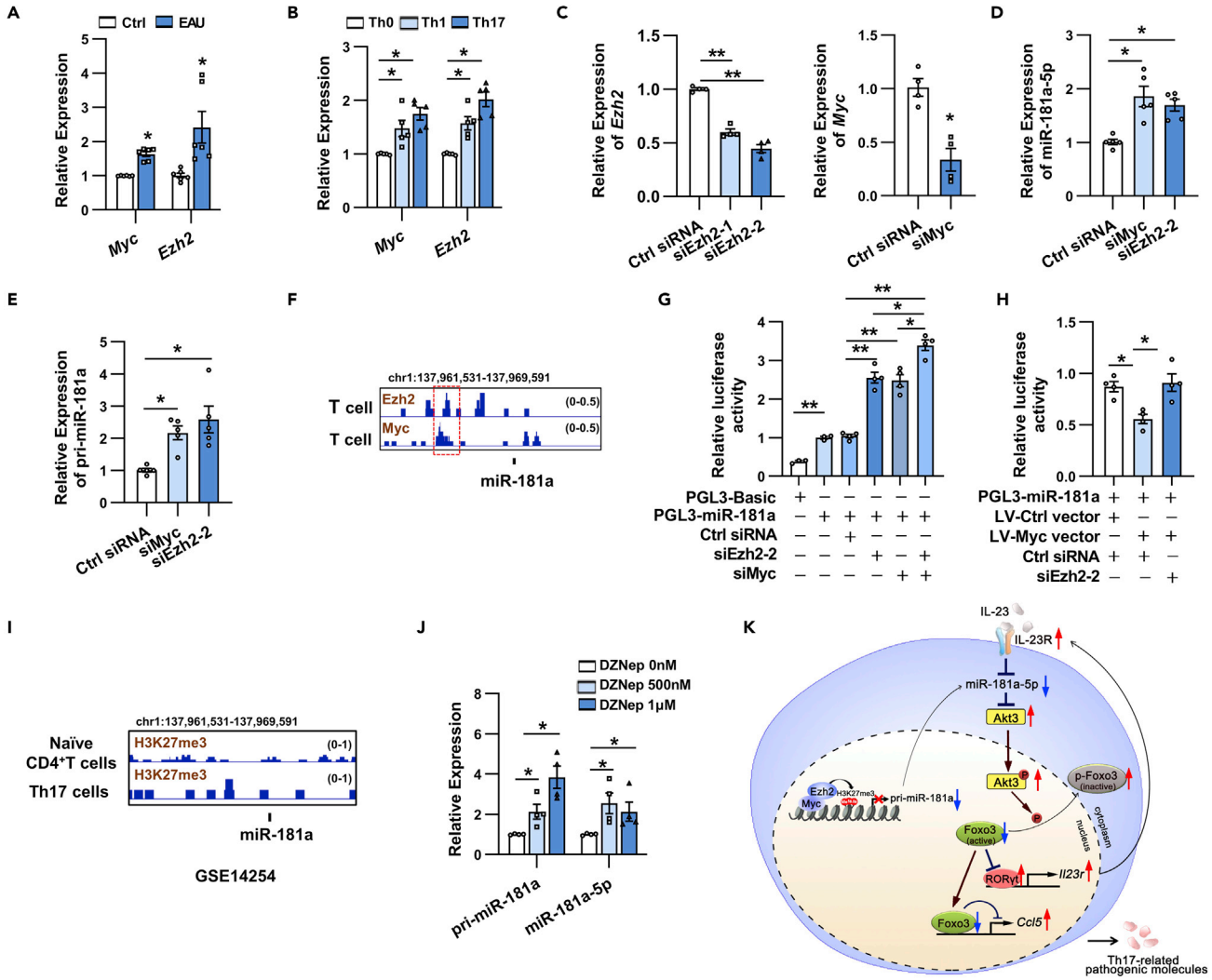

Figure 6. EZH2 and MYC cooperatively suppress miR-181a-5p expression in IRBP-specific Th17 cells

(A and B) Real-time qRT-PCR analysis of *Myc* and *Ezh2* expression in CD4$^+$ T cells from naive and EAU mice (A), or in EAU CD4$^+$ T cells cultured under Th0, Th1, or Th17 polarization conditions (B) (n = 5–6 per group).

(C–E) Real-time qRT-PCR analysis of *Myc*, *Ezh2*, pri-miR-181a, and miR-181a-5p expression in Th17 cells transfected with indicated oligonucleotides (n = 4–5 per group).

(F) MYC and EZH2 occupancy on the murine miR-181a locus were analyzed using the MYC and EZH2 ChIP-seq data of T cells from the Cistrome Project.

(G and H) Luciferase activity analysis of reporter containing *miR-181a* promoter co-transfected into EL4 T with the indicated plasmids (n = 3–4 per group).

(I) Genomic tracks displaying ChIP-seq data of CD4$^+$ naive T cells and Th17 cells for H3K27me3 histone modifications across the murine miR-181a region by analysis of the published ChIP-seq database (GSE14254).

(J) Real-time qRT-PCR analysis of pri-miR-181a and miR-181a-5p in IRBP-specific Th17 cells treated with or without DZNep (n = 4 per group).

(K) Illustration depicting how miR-181a-5p regulated pathogenic Th17 cell responses. Data are presented as mean ± SEM of at least three independent experiments. In the statistical analysis, Mann-Whitney U test (A), One-way ANOVA (B–E, and G and H), and Kruskal-Wallis test (J) were used with significance defined as *p<0.05, **p<0.01. See also Figures S5 and S6.

Th17 cells, and it inhibited pathogenic Th17 cell responses *in vivo* and *in vitro*. At the molecular level, miR-181a-5p directly targeted AKT3 to reduce the phosphorylation levels of AKT/FOXO3, leading to decreased IL-23R and CCL5 expression. Accordingly, both global and Th17 cell-specific overexpression of miR-181a-5p effectively protects mice against the development of EAU.

miR-181a-5p has been linked to the Th17 cell biology. It inhibited Th17 cell differentiation by targeting IFN-γ (Sang et al., 2015) in human CD4$^+$ T cells on anti-CD3/CD28 stimulation, decreased the frequency of Th17 cells by inhibiting HMGB1 or IL-2 expression in murine CD4$^+$ T cells (He et al., 2022;

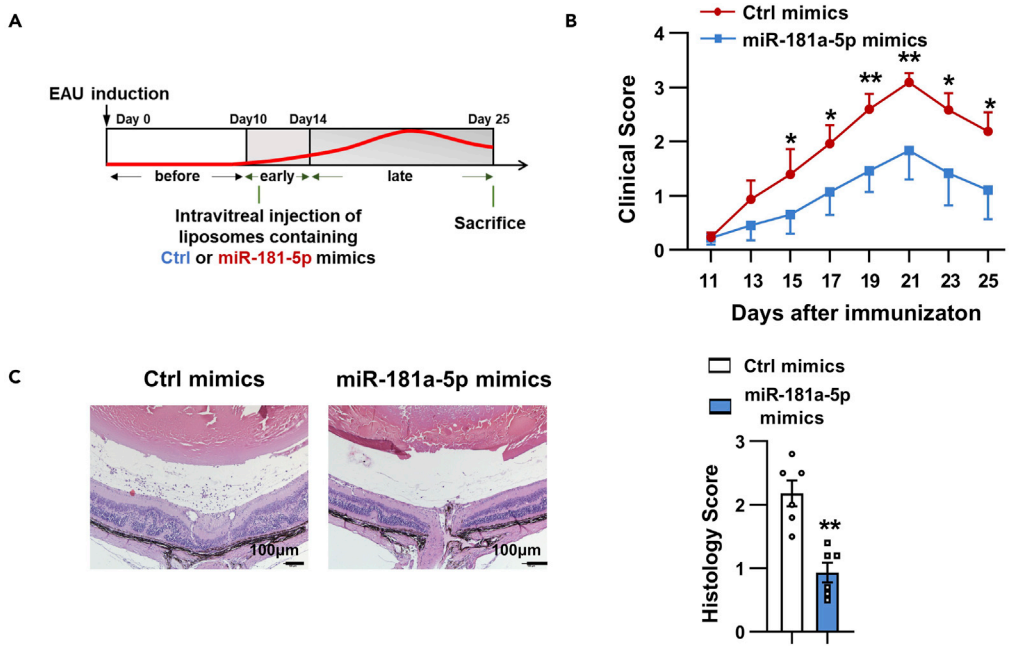

Figure 7. Local administration of miR-181a-5p mimics at the early phase of disease could ameliorate EAU

(A) Experimental protocol for the treatment of EAU by intravitreal injection of miR-181a-5p or Ctrl mimics.

(B and C) Clinical scores (B) and histopathological analysis (C) of EAU mice intravitreal injected with miR-181a-5p or Ctrl mimics (n = 6 mice per group). Scale bars, 100 μm. Error bars represent the mean ± SEM. In the statistical analysis, two-way ANOVA (B) and Student's t test (C) were used with significance defined as *p<0.05, **p<0.01.

Liu et al., 2019), and affected cell survival by modulating BCL-2 expression in Th17 cells (Song et al., 2018). Nonetheless, little is known with regard to the role of miR-181a-5p in pathogenic Th17 cells. Here, using combination of loss- and gain-of-function experiments, IRBP-induced or T cell transfer model of EAU, we demonstrated that miR-181a-5p suppressed pathogenic Th17 cell responses as well as the ability of Th17 cells to provoke EAU *in vivo* and *in vitro*. These data highlighted the importance of T cell-intrinsic miR-181a-5p in controlling pathogenic Th17 cell function and EAU. Enhanced miR-181a-5p expression may cause the decreased survival and proliferation of autoreactive Th17 cells, leading to alleviated EAU in miR-181a overexpressing mice. In addition, we observed a significant decrease in the expression of *Il23*, *Il6*, and *Il1b* in the spleens of LV-181a-infected EAU mice and miR-181a-5p-overexpressing dendritic cells (DCs) (Figures 2I and S3A). IL-23, IL-6, and IL-1β produced mainly by DCs are pathogenic Th17 cell instructive cytokines (Ghoreschi et al., 2010). IL-6 is essential for priming pathogenic Th17 cell responses (Heink et al., 2017), and IL-23 and IL-1β signaling can promote stabilization and expansion of pathogenic Th17 cells (Lee et al., 2012; Mufazalov et al., 2017). By reducing these cytokines, miR-181a-5p modulated DCs may create a cytokine milieu that indirectly suppresses the generation of pathogenic Th17 cells in EAU. Indeed, we found that miR-181a-5p-overexpressing DCs significantly decreased the expression of pathogenic Th17 signature genes and the percentages of Th17 cells *in vitro* (Figures S3B and S3C). Via inhibiting Th1-associated transcription factor *Tbx21* and cytokine IFN-γ, miR-181a-5p also dramatically repressed pathogenic Th1 responses, in line with previous studies showing that miR-181a-5p inhibited Th1 responses via targeting of IFN-γ *in vitro* (Sang et al., 2015). Given that both Th17 and Th1 cells are important mediators of uveitis (Luger et al., 2008), manipulation of miR-181a-5p expression may be a potential therapeutic strategy for uveitis treatment. Indeed, we observed that local administration of miR-181a-5p mimics effectively ameliorated the severity of established EAU.

Our further mechanism study showed that AKT3 is a functional target of miR-181a-5p in EAU, which is consistent with a recent study revealing that miR-181a-5p negatively regulated the expression of AKT3 in gastric adenocarcinoma (Lu et al., 2019). AKT3 deficient naive T cells exhibited a significantly increased efficiency of differentiation toward Th17 cells (DuBois et al., 2019). Nonetheless, AKT3 in control of antigen-specific Th17 cell responses has not been investigated. Here, we found that AKT3 silencing resulted in significantly decreased IL-17 production and reduced expression of pathogenic Th17 signature genes,

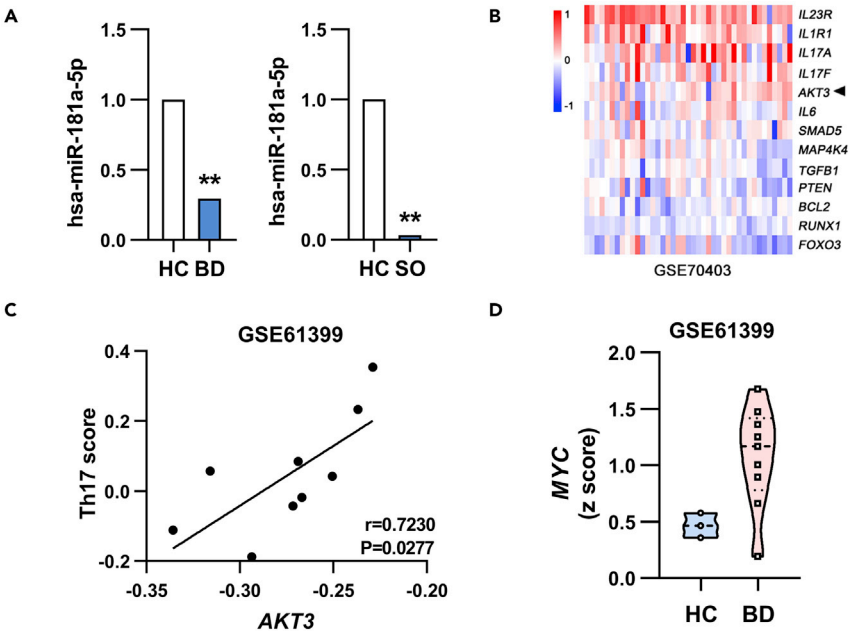

Figure 8. The MYC/miR-181a-5p/AKT3 pathway in uveitis patients

(A) Downregulated miR-181a-5p expression was shown in PBMCs from patients with BD (n = 6) (Puccetti et al., 2018) and enucleated globes of sympathetic ophthalmia (SO) (n = 4) (Kaneko et al., 2012). Reprinted by permission from Association for Research in Vision and Ophthalmology Publishers: Investigative Ophthalmology & Visual Science (Kaneko et al., 2012), Copyright 2012; and Hindnawi Publishers: Journal of Immunology Research (Puccetti et al., 2018), Copyright 2018.

(B) Upregulated *AKT3* expression was shown in PBMCs from BD patients by analysis of clinical dataset GSE70403(41 patients with BD and 17 normal volunteers).

(C) Correlation between *AKT3* gene expression and Th17 score in $CD4^+$ T cells of BD patients was analyzed by the Pearson correlation test. The Th17 score was calculated based on the average expression level of *IL-17*, *RORC*, *IL-23R*, *GM-CSF* and *CCL5* genes (n = 9).

(D) Upregulated *MYC* expression was shown in $CD4^+$ T cells of BD patients by analysis of clinical dataset GSE61399 (9 patients with BD and 3 healthy controls). The *Z* score transformed values of the microarray gene expression dataset GSE70403 (B) and GSE61399 (C, D). *p<0.05, **p<0.01.

suggesting that AKT3 functions as a T cell-intrinsic positive regulator of pathogenic Th17 cells. Compatible with our observation is the data that AKT3 expression correlated positively with the expression of pathogenic Th17 signature genes in uveitis patients, implicating the importance of AKT3 in human Th17-driven autoimmunity. Importantly, we also found that AKT3 silencing partially reversed increased pathogenic Th17-related gene expression induced by miR-181a-5p inhibitor in Th17 cells, indicating the involvement of AKT3 signaling in miR-181a-5p-mediated defective pathogenic Th17 responses. However, we cannot exclude the involvement of other mechanisms. For instance, miR-181a-5p can modulate ERK signaling to favor human memory Th17 cell activation (Mele et al., 2015). Whether miR-181a-5p could regulate pathogenic Th17 responses via ERK signaling in EAU remained to be determined.

FOXO3, one main member of the FOXO transcription factor family, is a key downstream target of AKT signaling. It has been shown to promote Treg generation by facilitating TGF-β-induced Foxp3 expression via binding to its locus (Ouyang et al., 2010), and drive pathogenic Th1 cell differentiation by inducing Eomes expression (Stienne et al., 2016). However, the role played by FOXO3 in Th17 responses is less well defined. IL-23/IL-23R signaling was important for the stability and function of pathogenic Th17 cells (Wu et al., 2013). Here, using luciferase reporters containing *Il23r* promoter region, we demonstrated that FOXO3 inhibited the transcription of *Il23r* via interference of RORγt activity. CCL5, a key chemokine that can expand Th17 cell-mediated autoimmune pathogenesis via recruiting inflammatory cells into intraocular inflammatory sites (Niu et al., 2019), is among the genes that highly expressed in human and murine pathogenic Th17 cells (Hu et al., 2017). Moreover, CCL5 has been reported to be elevated in the aqueous humor and vitreous of patients with autoimmune uveitis and correlated with the clinical severity of the disease (Adamus et al., 2001; Fukunaga et al., 2020), further supporting the role of this chemokine in human ocular inflammation. In vascular smooth muscle cells, NF-κB and STAT3 interacted to

modulate CCL5 transcription (Kovacic et al., 2010). Moreover, ASIC1a enhanced CCL5 expression by inducing nuclear translocation of NFATc3 in rheumatoid arthritis synovial fibroblasts (Zhang et al., 2020). Our findings that FOXO3 repressed CCL5 expression by directly binding to its promoter region add another layer of complexity to the CCL5 regulatory network. In addition, the promoter region of *Il17a* gene has several putative FOXO3-binding sites (FBS) (Figure S4A), meaning that it can be modulated directly by FOXO3. Collectively, FOXO3 might control the pathogenicity of Th17 cells to act on not only IL-23R but also CCL5 or others.

$FOXP3^+$ Treg cells suppress inflammation and control the development of various autoimmune diseases including uveitis. IL-10 and TGF-β released by Tregs directly mediate their inhibitory function. Recently, AHR has been demonstrated to inhibit the enrichment of histone H3K9me3 at *Foxp3* promoter region and promote the expression of FOXP3 and IL-10 (Lv et al., 2018). Here, we observed a significant increase not only in the percentage of Treg cells but also in the expression of Treg-related genes in the T cells from miR-181a-overexpressing mice, suggesting that miR-181a-5p may augment Treg cell differentiation and function. Our results are supported by previous studies showing that miR-181a promoted Treg differentiation through targeting SMAD7 *in vitro* (Ghorbani et al., 2017), and miR-181a deficiency impaired the generation of Tregs via elevating the expression of CTLA4 in thymus (Lyszkiewicz et al., 2019). In contrast, Serr et al. (2018) reported that miR-181a mimics impeded human and murine Treg induction by enhancing NFAT5 expression. Further studies are needed to define the molecular mechanisms underlying modulation of Tregs by miR-181a -5p in EAU.

Aberrant miRs expression has been reported in uveitis (Kaneko et al., 2012; Muhammad et al., 2019; Puccetti et al., 2018; Wei et al., 2019). However, the molecular basis for miR dysregulation remains unclear. EZH2 is the histone methyltransferase that catalyzes H3K27me3, thereby mediating epigenetic gene silencing (Baer et al., 2013). Recent studies have shown that MYC is essential for recruiting EZH2 to the regulatory regions of miRs, which further mediate H3K27me3 and induce silencing of tumor suppressive miRs (Wang et al., 2014; Zhang et al., 2018). In this study, we revealed that MYC was highly expressed in IRBP-specific Th17 cells and positively regulated Th17 responses (Figures 6A and S5A–S5D), in line with a previous study in EAE showing that the pharmacological inhibition of MYC resulted in significantly decreased IL-17 production (Bandukwala et al., 2012). Furthermore, we found that MYC and EZH2 might act in concert to epigenetically silence miR-181a-5p expression in IRBP-specific Th17 cells, implying the important role of MYC in EAU progression that warrants further study. In the endometrial cancer cell, lncRNA DLEU2 interacted with EZH2 to inhibit hsa-miR-181a expression (Dong et al., 2021), suggesting the complexity of the molecular regulatory networks underlying miR-181a dysregulation. Of note, a study from Shi et al. (2018) reported that miR-181a was silenced in human colorectal cancer because of DNA hypermethylation. In contrast, we did not observe statistical difference in levels of miR-181a-5p between DNA methyltransferases inhibitor treated and untreated Th17 cells (Figure S6A). Differences in species and cell types may account for the discrepancy in these studies. Future studies should define how MYC and EZH2 cooperatively control miR-181a-5p expression in the progression of EAU.

In summary, our findings elucidated a critical function for miR-181a-5p in attenuating Th17 cell-mediated autoimmunity. miR-181a-5p directly targets AKT3, which activates AKT3-regulated transcription factor activity of FOXO3, leading to decreased pathogenic Th17 cell responses. These findings shed new light on uveitis mechanisms and might guide the development of effective therapeutics for uveitis and other Th17-mediated autoimmune diseases.

Limitations of the study

In this study, we perform extensive *in vitro* and *in vivo* experiments to prove that miR-181a-5p negatively regulates pathogenic Th17 cell functions via modulating AKT3/FOXO3 signaling. However, we cannot rule out the involvement of other signaling pathways. Also, detailed study is necessary to define how MYC and EZH2 cooperatively control miR-181a-5p expression in pathogenic Th17 cells in EAU. In addition, miR-181a-5p shows promising therapeutic effects in EAU, whereas the comparable effects remain to be assessed in human studies.

STAR★METHODS

Detailed methods are provided in the online version of this paper and include the following:

- KEY RESOURCES TABLE
- RESOURCE AVAILABILITY
  - Lead contact

SUPPLEMENTAL INFORMATION

Supplemental information can be found online at https://doi.org/10.1016/j.isci.2022.105176.

ACKNOWLEDGMENTS

We thank Dr. Zhuqiang Zhang (Institute of Biophysics, Chinese Academy of Sciences) for expert advice and critical review of the manuscript. We thank Prof. Chunsheng Han and Dr. Jian Chen (Institute of Zoology, Chinese Academy of Science) for providing reagents. We thank Dr. Zhihui Zhang for technical assistance. This work was supported by the National Natural Science Foundation of China (81970793, 82070929, 81870675), and the Tianjin Clinical Key Discipline Project (TJLCZDXKT003).

AUTHOR CONTRIBUTIONS

H.N. conceived and supervised the study. H.N., X.L. and R.W. were responsible for securing funding. H.N., X.L., S.C., and B.M. designed the experiments. S.C., X.L., K.Z., Y.W., B.D., and X.L. performed the experiments. S.C., B.M., X.L., K.Z., and Y.W. analyzed the data. H.N., S.C., and B.M. wrote the manuscript with input from all the authors.

DECLARATION OF INTERESTS

The authors declare no competing interests.

Received: April 6, 2022
Revised: August 18, 2022
Accepted: September 16, 2022
Published: October 21, 2022

REFERENCES

Adamus, G., Manczak, M., and Machnicki, M. (2001). Expression of CC chemokines and their receptors in the eye in autoimmune anterior uveitis associated with EAE. Invest. Ophthalmol. Vis. Sci. *42*, 2894–2903.

Agarwal, R.K., Silver, P.B., and Caspi, R.R. (2012). Rodent models of experimental autoimmune uveitis. Methods Mol. Biol. *900*, 443–469. https://doi.org/10.1007/978-1-60761-720-4_22.

Amadi-Obi, A., Yu, C.R., Liu, X., Mahdi, R.M., Clarke, G.L., Nussenblatt, R.B., Gery, I., Lee, Y.S., and Egwuagu, C.E. (2007). TH17 cells contribute to uveitis and scleritis and are expanded by IL-2 and inhibited by IL-27/STAT1. Nat. Med. *13*, 711–718. https://doi.org/10.1038/nm1585.

Baer, C., Claus, R., and Plass, C. (2013). Genome-wide epigenetic regulation of miRNAs in cancer. Cancer Res. *73*, 473–477. https://doi.org/10.1158/0008-5472.CAN-12-3731.

Bandukwala, H.S., Gagnon, J., Togher, S., Greenbaum, J.A., Lamperti, E.D., Parr, N.J., Molesworth, A.M.H., Smithers, N., Lee, K., Witherington, J., et al. (2012). Selective inhibition

of CD4+ T-cell cytokine production and autoimmunity by BET protein and c-Myc inhibitors. Proc. Natl. Acad. Sci. USA *109*, 14532–14537. https://doi.org/10.1073/pnas.1212264109.

Bi, J., Zeng, X., Zhao, L., Wei, Q., Yu, L., Wang, X., Yu, Z., Cao, Y., Shan, F., and Wei, M. (2016). miR-181a induces macrophage polarized to M2 phenotype and promotes M2 macrophage-mediated tumor cell metastasis by targeting KLF6 and C/EBPalpha. Mol. Ther. Nucleic Acids *5*, e368. https://doi.org/10.1038/mtna.2016.71.

Bowers, C.E., Calder, V.L., Greenwood, J., and Eskandarpour, M. (2022). Experimental autoimmune uveitis: an intraocular inflammatory mouse model. J. Vis. Exp. *179*. https://doi.org/10.3791/61832.

Chong, W.P., Mattapallil, M.J., Raychaudhuri, K., Bing, S.J., Wu, S., Zhong, Y., Wang, W., Chen, Z., Silver, P.B., Jittayasothorn, Y., et al. (2020). The cytokine IL-17alimits Th17 pathogenicity via a negative feedback loop driven by autocrine induction of IL-24. Immunity *53*, 384–397.e5. https://doi.org/10.1016/j.immuni.2020.06.022.

Dong, P., Xiong, Y., Konno, Y., Ihira, K., Kobayashi, N., Yue, J., and Watari, H. (2021). Long non-coding RNA DLEU2 drives EMT and glycolysis in endometrial cancer through HK2 by competitively binding with miR-455 and by modulating the EZH2/miR-181a pathway. J. Exp. Clin. Cancer Res. *40*, 216. https://doi.org/10.1186/s13046-021-02018-1.

Du, C., Liu, C., Kang, J., Zhao, G., Ye, Z., Huang, S., Li, Z., Wu, Z., and Pei, G. (2009). MicroRNA miR-326 regulates TH-17 differentiation and is associated with the pathogenesis of multiple sclerosis. Nat. Immunol. *10*, 1252–1259. https://doi.org/10.1038/ni.1798.

DuBois, J.C., Ray, A.K., Gruber, R.C., Zhang, Y., Aflakpui, R., Macian-Juan, F., and Shafit-Zagardo, B. (2019). Akt3-Mediated protection against inflammatory demyelinating disease. Front. Immunol. *10*, 1738. https://doi.org/10.3389/fimmu.2019.01738.

Fukunaga, H., Kaburaki, T., Shirahama, S., Tanaka, R., Murata, H., Sato, T., Takeuchi, M., Tozawa, H., Urade, Y., Katsura, M., et al. (2020). Analysis of inflammatory mediators in the vitreous humor of eyes with pan-uveitis according to aetiological classification. Sci. Rep. *10*, 2783. https://doi.org/10.1038/s41598-020-59666-0.

Ghorbani, S., Talebi, F., Chan, W.F., Masoumi, F., Vojgani, M., Power, C., and Noorbakhsh, F. (2017). MicroRNA-181 variants regulate T cell phenotype in the context of autoimmune neuroinflammation. Front. Immunol. *8*, 758. https://doi.org/10.3389/fimmu.2017.00758.

Ghoreschi, K., Laurence, A., Yang, X.P., Tato, C.M., McGeachy, M.J., Konkel, J.E., Ramos, H.L., Wei, L., Davidson, T.S., Bouladoux, N., et al. (2010). Generation of pathogenic T(H)17 cells in the absence of TGF-beta signalling. Nature *467*, 967–971. https://doi.org/10.1038/nature09447.

Griffiths-Jones, S., Saini, H.K., van Dongen, S., and Enright, A.J. (2008). miRBase: tools for microRNA genomics. Nucleic Acids Res. *36*, D154–D158. https://doi.org/10.1093/nar/gkm952.

He, R., Chen, Y., Chen, X., and Yuan, B. (2022). Mechanism of miR-181a-5p in regulatory T/T-Helper 17 immune imbalance and asthma development in mice with allergic rhinitis. Int. Arch. Allergy Immunol. *183*, 375–388. https://doi.org/10.1159/000519703.

Heink, S., Yogev, N., Garbers, C., Herwerth, M., Aly, L., Gasperi, C., Husterer, V., Croxford, A.L., Möller-Hackbarth, K., Bartsch, H.S., et al. (2017). Trans-presentation of IL-6 by dendritic cells is required for the priming of pathogenic TH17 cells. Nat. Immunol. *18*, 74–85. https://doi.org/10.1038/ni.3632.

Hu, D., Notarbartolo, S., Croonenborghs, T., Patel, B., Cialic, R., Yang, T.H., Aschenbrenner, D., Andersson, K.M., Gattorno, M., Pham, M., et al. (2017). Transcriptional signature of human pro-inflammatory TH17 cells identifies reduced IL10 gene expression in multiple sclerosis. Nat. Commun. *8*, 1600. https://doi.org/10.1038/s41467-017-01571-8.

Ichiyama, K., Gonzalez-Martin, A., Kim, B.S., Jin, H.Y., Jin, W., Xu, W., Sabouri-Ghomi, M., Xu, S., Zheng, P., Xiao, C., and Dong, C. (2016). The MicroRNA-183-96-182 cluster promotes T helper 17 cell pathogenicity by negatively regulating transcription factor Foxo1 expression. Immunity *44*, 1284–1298. https://doi.org/10.1016/j.immuni.2016.05.015.

Kaneko, Y., Wu, G.S., Saraswathy, S., Vasconcelos-Santos, D.V., and Rao, N.A. (2012). Immunopathologic processes in sympathetic ophthalmia as signified by microRNA profiling. Invest. Ophthalmol. Vis. Sci. *53*, 4197–4204. https://doi.org/10.1167/iovs.12-9465.

Kim, C., Ye, Z., Weyand, C.M., and Goronzy, J.J. (2021). miR-181a-regulated pathways in T-cell differentiation and aging. Immun. Ageing *18*, 28. https://doi.org/10.1186/s12979-021-00240-1.

Kovacic, J.C., Gupta, R., Lee, A.C., Ma, M., Fang, F., Tolbert, C.N., Walts, A.D., Beltran, L.E., San, H., Chen, G., et al. (2010). Stat3-dependent acute Rantes production in vascular smooth muscle cells modulates inflammation following arterial injury in mice. J. Clin. Invest. *120*, 303–314. https://doi.org/10.1172/JCI40364.

Lee, Y., Awasthi, A., Yosef, N., Quintana, F.J., Xiao, S., Peters, A., Wu, C., Kleinewietfeld, M., Kunder, S., Hafler, D.A., et al. (2012). Induction and molecular signature of pathogenic TH17 cells. Nat. Immunol. *13*, 991–999. https://doi.org/10.1038/ni.2416.

Liu, X., Luo, M., Meng, H., Zeng, Q., Xu, L., Hu, B., Luo, Y., Liu, C., Luo, Z., and Yang, H. (2019). MiR-181a regulates CD4(+) T cell activation and differentiation by targeting IL-2 in the pathogenesis of myasthenia gravis. Eur. J. Immunol. eji.201848007. https://doi.org/10.1002/eji.201848007.

Lu, Z., Luo, T., Pang, T., Du, Z., Yin, X., Cui, H., Fang, G., and Xue, X. (2019). MALAT1 promotes gastric adenocarcinoma through the MALAT1/miR-181a-5p/AKT3 axis. Open Biol. *9*, 190095. https://doi.org/10.1098/rsob.190095.

Luger, D., Silver, P.B., Tang, J., Cua, D., Chen, Z., Iwakura, Y., Bowman, E.P., Sgambellone, N.M., Chan, C.C., and Caspi, R.R. (2008). Either a Th17 or a Th1 effector response can drive autoimmunity: conditions of disease induction affect dominant effector category. J. Exp. Med. *205*, 799–810. https://doi.org/10.1084/jem.20071258.

Lutz, M.B., Kukutsch, N., Ogilvie, A.L., Rössner, S., Koch, F., Romani, N., and Schuler, G. (1999). An advanced culture method for generating large quantities of highly pure dendritic cells from mouse bone marrow. J. Immunol. Methods *223*, 77–92. https://doi.org/10.1016/s0022-1759(98)00204-x.

Lv, Q., Wang, K., Qiao, S., Yang, L., Xin, Y., Dai, Y., and Wei, Z. (2018). Norisoboldine, a natural AhR agonist, promotes Treg differentiation and attenuates colitis via targeting glycolysis and subsequent NAD(+)/SIRT1/SUV39H1/H3K9me3 signaling pathway. Cell Death Dis. *9*, 258. https://doi.org/10.1038/s41419-018-0297-3.

Łyszkiewicz, M., Winter, S.J., Witzlau, K., Föhse, L., Brownlie, R., Puchałka, J., Verheyden, N.A., Kunze-Schumacher, H., Imelmann, E., Blume, J., et al. (2019). miR-181a/b-1 controls thymic selection of Treg cells and tunes their suppressive capacity. PLoS Biol. *17*, e2006716. https://doi.org/10.1371/journal.pbio.2006716.

Manning, B.D., and Toker, A. (2017). AKT/PKB signaling: navigating the network. Cell *169*, 381–405. https://doi.org/10.1016/j.cell.2017.04.001.

McGeachy, M.J., Bak-Jensen, K.S., Chen, Y., Tato, C.M., Blumenschein, W., McClanahan, T., and Cua, D.J. (2007). TGF-beta and IL-6 drive the production of IL-17 and IL-10 by T cells and restrain T(H)-17 cell-mediated pathology. Nat. Immunol. *8*, 1390–1397. https://doi.org/10.1038/ni1539.

Mehta, A., and Baltimore, D. (2016). MicroRNAs as regulatory elements in immune system logic. Nat. Rev. Immunol. *16*, 279–294. https://doi.org/10.1038/nri.2016.40.

Mele, F., Basso, C., Leoni, C., Aschenbrenner, D., Becattini, S., Latorre, D., Lanzavecchia, A., Sallusto, F., and Monticelli, S. (2015). ERK phosphorylation and miR-181a expression modulate activation of human memory TH17 cells. Nat. Commun. *6*, 6431. https://doi.org/10.1038/ncomms7431.

Mufazalov, I.A., Schelmbauer, C., Regen, T., Kuschmann, J., Wanke, F., Gabriel, L.A., Hauptmann, J., Müller, W., Pinteaux, E., Kurschus, F.C., and Waisman, A. (2017). IL-1 signaling is critical for expansion but not generation of autoreactive GM-CSF+ Th17 cells. EMBO J. *36*, 102–115. https://doi.org/10.15252/embj.201694615.

Muhammad, F., Trivett, A., Wang, D., and Lee, D.J. (2019). Tissue-specific production of MicroRNA-155 inhibits melanocortin 5 receptor-dependent suppressor macrophages to promote experimental autoimmune uveitis. Eur. J. Immunol. *49*, 2074–2082. https://doi.org/10.1002/eji.201848073.

Mycko, M.P., Cichalewska, M., Machlanska, A., Cwiklinska, H., Mariasiewicz, M., and Selmaj, K.W. (2012). MicroRNA-301a regulation of a T-helper 17 immune response controls autoimmune demyelination. Proc. Natl. Acad. Sci. USA *109*, E1248–E1257. https://doi.org/10.1073/pnas.1114325109.

Nian, H., Liang, D., Zuo, A., Wei, R., Shao, H., Born, W.K., Kaplan, H.J., and Sun, D. (2012). Characterization of autoreactive and bystander IL-17+ T cells induced in immunized C57BL/6 mice. Invest. Ophthalmol. Vis. Sci. *53*, 897–905. https://doi.org/10.1167/iovs.11-8297.

Niu, T., Cheng, L., Wang, H., Zhu, S., Yang, X., Liu, K., Jin, H., and Xu, X. (2019). KS23, a novel peptide derived from adiponectin, inhibits retinal inflammation and downregulates the proportions of Th1 and Th17 cells during experimental autoimmune uveitis. J. Neuroinflammation *16*, 278. https://doi.org/10.1186/s12974-019-1686-y.

O'Connell, R.M., Rao, D.S., Chaudhuri, A.A., and Baltimore, D. (2010). Physiological and pathological roles for microRNAs in the immune system. Nat. Rev. Immunol. *10*, 111–122. https://doi.org/10.1038/nri2708.

Ouyang, W., Beckett, O., Ma, Q., Paik, J.H., DePinho, R.A., and Li, M.O. (2010). Foxo proteins cooperatively control the differentiation of Foxp3+ regulatory T cells. Nat. Immunol. *11*, 618–627. https://doi.org/10.1038/ni.1884.

Puccetti, A., Pelosi, A., Fiore, P.F., Patuzzo, G., Lunardi, C., and Dolcino, M. (2018). MicroRNA expression profiling in behcet's disease. J. Immunol. Res. *2018*, 2405150. https://doi.org/10.1155/2018/2405150.

Sang, W., Zhang, C., Zhang, D., Wang, Y., Sun, C., Niu, M., Sun, X., Zhou, C., Zeng, L., Pan, B., et al. (2015). MicroRNA-181a, a potential diagnosis marker, alleviates acute graft versus host disease by regulating IFN-gamma production. Am. J. Hematol. *90*, 998–1007. https://doi.org/10.1002/ajh.24136.

Serr, I., Scherm, M.G., Zahm, A.M., Schug, J., Flynn, V.K., Hippich, M., Kälin, S., Becker, M., Achenbach, P., Nikolaev, A., et al. (2018). A miRNA181a/NFAT5 axis links impaired T cell tolerance induction with autoimmune type 1 diabetes. Sci. Transl. Med. *10*, eaag1782. https://doi.org/10.1126/scitranslmed.aag1782.

Shao, H., Liao, T., Ke, Y., Shi, H., Kaplan, H.J., and Sun, D. (2006). Severe chronic experimental autoimmune uveitis (EAU) of the C57BL/6 mouse induced by adoptive transfer of IRBP1-20-specific T cells. Exp. Eye Res. *82*, 323–331. https://doi.org/10.1016/j.exer.2005.07.008.

Shi, L., Li, X., Wu, Z., Li, X., Nie, J., Guo, M., Mei, Q., and Han, W. (2018). DNA methylation-mediated repression of miR-181a/135a/302c expression promotes the microsatellite-unstable colorectal cancer development and 5-FU resistance via targeting PLAG1. J. Genet. Genom. *45*, 205–214. https://doi.org/10.1016/j.jgg.2018.04.003.

Singh, U.P., Murphy, A.E., Enos, R.T., Shamran, H.A., Singh, N.P., Guan, H., Hegde, V.L., Fan, D., Price, R.L., Taub, D.D., et al. (2014). miR-155 deficiency protects mice from experimental colitis by reducing T helper type 1/type 17 responses. Immunology *143*, 478–489. https://doi.org/10.1111/imm.12328.

Song, Y., Yang, H., Jiang, K., Wang, B.M., and Lin, R. (2018). miR-181a regulates Th17 cells distribution via up-regulated BCL-2 in primary biliary cholangitis. Int. Immunopharmacol. *64*, 386–393. https://doi.org/10.1016/j.intimp.2018.09.027.

Stienne, C., Michieletto, M.F., Benamar, M., Carrié, N., Bernard, I., Nguyen, X.H., Lippi, Y., Duguet, F., Liblau, R.S., Hedrick, S.M., et al. (2016). Foxo3 transcription factor drives pathogenic T helper 1 differentiation by inducing the expression of Eomes. Immunity *45*, 774–787. https://doi.org/10.1016/j.immuni.2016.09.010.

Sun, Y., Liu, C.H., SanGiovanni, J.P., Evans, L.P., Tian, K.T., Zhang, B., Stahl, A., Pu, W.T., Kamenecka, T.M., Solt, L.A., and Chen, J. (2015). Nuclear receptor RORalpha regulates pathologic retinal angiogenesis by modulating SOCS3-dependent inflammation. Proc. Natl. Acad. Sci. USA *112*, 10401–10406. https://doi.org/10.1073/pnas.1504387112.

Valencia, K., Erice, O., Kostyrko, K., Hausmann, S., Guruceaga, E., Tathireddy, A., Flores, N.M., Sayles, L.C., Lee, A.G., Fragoso, R., et al. (2020). The Mir181ab1 cluster promotes KRAS-driven oncogenesis and progression in lung and pancreas. J. Clin. Invest. *130*, 1879–1895. https://doi.org/10.1172/JCI129012.

Wang, L., Zhang, X., Jia, L.T., Hu, S.J., Zhao, J., Yang, J.D., Wen, W.H., Wang, Z., Wang, T., Zhao, J., et al. (2014). c-Myc-mediated epigenetic silencing of MicroRNA-101 contributes to dysregulation of multiple pathways in hepatocellular carcinoma. Hepatology *59*, 1850–1863. https://doi.org/10.1002/hep.26720.

Wei, Y., Chen, S., Sun, D., Li, X., Wei, R., Li, X., and Nian, H. (2019). miR-223-3p promotes autoreactive Th17 cell responses in experimental autoimmune uveitis (EAU) by inhibiting transcription factor FOXO3 expression. FASEB J. *33*, 13951–13965. https://doi.org/10.1096/fj.201901446R.

Wu, C., Yosef, N., Thalhamer, T., Zhu, C., Xiao, S., Kishi, Y., Regev, A., and Kuchroo, V.K. (2013). Induction of pathogenic TH17 cells by inducible salt-sensing kinase SGK1. Nature *496*, 513–517. https://doi.org/10.1038/nature11984.

Xiang, Y., Cheng, J., Wang, D., Hu, X., Xie, Y., Stitham, J., Atteya, G., Du, J., Tang, W.H., Lee, S.H., et al. (2015). Hyperglycemia repression of miR-24 coordinately upregulates endothelial cell expression and secretion of von Willebrand factor. Blood *125*, 3377–3387. https://doi.org/10.1182/blood-2015-01-620278.

Zhang, X., Zhang, X., Wang, T., Wang, L., Tan, Z., Wei, W., Yan, B., Zhao, J., Wu, K., Yang, A., et al. (2018). MicroRNA-26a is a key regulon that inhibits progression and metastasis of c-Myc/EZH2 double high advanced hepatocellular carcinoma. Cancer Lett. *426*, 98–108. https://doi.org/10.1016/j.canlet.2018.04.005.

Zhang, Y., Qian, X., Yang, X., Niu, R., Song, S., Zhu, F., Zhu, C., Peng, X., and Chen, F. (2020). ASIC1a induces synovial inflammation via the Ca(2+)/NFATc3/RANTES pathway. Theranostics *10*, 247–264. https://doi.org/10.7150/thno.37200.

Zhong, Z., Su, G., Kijlstra, A., and Yang, P. (2021). Activation of the interleukin-23/interleukin-17 signalling pathway in autoinflammatory and autoimmune uveitis. Prog. Retin. Eye Res. *80*, 100866. https://doi.org/10.1016/j.preteyeres.2020.100866.

STAR★METHODS

KEY RESOURCES TABLE

REAGENT or RESOURCE	SOURCE	IDENTIFIER
Antibodies		
PE anti-mouse CD4	Biolegend	Cat#100408; RRID:AB_312693
FITC anti-mouse CD4	Biolegend	Cat#130308; RRID:AB_1279237
FITC anti-mouse IL-17A	Biolegend	Cat#506908; RRID:AB_536010
PE anti-mouse FOXP3	eBioscience	Cat#12-5773-82; RRID:AB_465936
Anti-AKT3	Cell Signaling Technology	Cat#3788; RRID:AB_2242534
Anti-Phospho-Akt	Cell Signaling Technology	Cat#12694; RRID:AB_2797994
Anti-FOXO3	Cell Signaling Technology	Cat#2497
Anti-Phospho-FOXO3	Cell Signaling Technology	Cat#9464; RRID:AB_329842
Anti-β-actin	Santa Cruz Biotechnology	Cat#sc47778; RRID:AB_626632
TruStain FcX™ PLUS (anti-mouse CD16/32) Antibody	Biolengent	Cat#156603; RRID:AB_2783137
Goat anti-rabbit Alexa Fluor® 594	Abcam	Cat#ab150080; RRID:AB_2650602
Horseradish Peroxidase-Conjugated Goat anti-Rabbit IgG	ZSGB-BIO	Cat#ZB-2301; RRID:AB_2747412
Horseradish Peroxidase-Conjugated Goat anti-Mouse IgG	ZSGB-BIO	Cat# ZB-2305; RRID:AB_2747415
Bacterial and virus strains		
Mycobacterium tuberculosis strain H37RA	BD Bioscience	Cat#231141
Chemicals, peptides, and recombinant proteins		
RPMI Medium 1640 basic	Gibco	Cat#C11875500BT
DMEM basic	Gibco	Cat#C1995500BT
Fetal bovine serum	HyClone	Cat#SH30406.05
β-mercaptoethanol	Gibco	Cat#21985023
Penicillin-streptomycin	Gibco	Cat#15140122
L-Glutamine	Gibco	Cat#A2916801
Lipofectamine 2000	Thermo Fisher Scientific	Cat#11668019
Lipopolysaccharide	InvivoGen	Cat#tlrl-eklps
PEG8000	Solarbio	Cat#P8260
TritonX-100	Solarbio	Cat#T8200
5% goat serum	Solarbio	Cat#SL038
Complete Freund's adjuvant (CFA)	Sigma-Aldrich, Merck	Cat#F5881
Pertussis toxin	Sigma-Aldrich, Merck	Cat#P7208
Phorbol myristate acetate	Sigma-Aldrich, Merck	Cat#P8139
Ionomycin	Sigma-Aldrich, Merck	Cat#407951
Brefeldin A	Sigma-Aldrich, Merck	Cat#B5936
Substrate Reagent Pack	R&D systems	Cat#DY999
IRBP peptide$_{1-20}$	Sangon Biotech	N/A
Recombinant mouse IL-4 protein	R&D systems	Cat#404-ML
Recombinant mouse IL-4 protein	R&D systems	Cat#419-ML
Recombinant mouse IL-23 protein	R&D systems	Cat#1887-ML
Recombinant mouse GM-CSF protein	R&D systems	Cat#415-ML

(*Continued on next page*)

Continued

REAGENT or RESOURCE	SOURCE	IDENTIFIER
Anti-PE MicroBeads	Miltenyi Biotec	Cat#130-048-801
Critical commercial assays		
Fixation and Permeabilization kit	eBioscience	Cat#00-5123
Mouse IL-17 DuoSet ELISA kits	R&D systems	Cat#DY421
Mouse IFN-gamma DuoSet ELISA kits	R&D systems	Cat#DY485
Dual Luciferase Reporter Assay kit	Promega	Cat#E1910
RevertAid First Strand cDNA Synthesis Kit	Thermo Fisher Scientific	Cat#K1622
FastStart SYBR Green Master Mix kit	Roche	Cat#04913914001
SDS-PAGE Gel Kit	Solarbio	Cat#P1200
Bicinchoninic Acid Assay Kit	Solarbio	Cat#PC0020
ECL reagent Kit	Cytiva	Cat#RPN2232
Deposited data		
Microarray profiles	GEO database	GSE213034
Original data	This paper; Mendeley Data	https://doi.org/10.17632/dp645s39h6.1
Experimental models: Cell lines		
HEK293T cells	ATCC	RRID:CVCL 0063
EL4 T cells	Chinese Academy of Science.	N/A
Experimental models: Organisms/strains		
C57BL/6 mice	Vital River Laboratory Animal Technology	RRID:MGI:2159769
Oligonucleotides		
Primers for qPCR, see supplemental information	This paper	N/A
miR-181a-5p mimics 5′-AACAUUCAACGCUGUCGGUGAGU-3′	Gene Pharma	N/A
Ctrl mimics 5′-UUCUUCGAACGUGUCACGU-3′	Gene Pharma	N/A
miR-181a-5p inhibitor 5′-ACUCACCGACAGCGUUGAAUGUU-3′	Gene Pharma	N/A
Ctrl inhibitor 5′-CAGUACUUUUGUGUAGUACAA-3′	Gene Pharma	N/A
siRNA-Myc 5′-GAACAUCAUCAUCCAGGAC-3′	Gene Pharma	N/A
siRNA-Akt3 5′-GGAUGAAGUGGCACACACU-3′	Gene Pharma	N/A
siRNA-Ezh2-1 5′-GCAGCUUUCUGUUCAACUU-3′	Gene Pharma	N/A
siRNA-Ezh2-2 5′-GGUGGAAGACGAAACUGUU-3′	Gene Pharma	N/A
Ctrl siRNA 5′-UUCUUCGAACGUGUCACGU-3′	Gene Pharma	N/A
Recombinant DNA		
pMIR-Report vector	Promega	N/A
pMIR-Akt3-WT	This paper	N/A
pMIR-Akt3-mut	This paper	N/A
pRL-TK vector	Promega	Cat#E2241

(*Continued on next page*)

Continued

REAGENT or RESOURCE	SOURCE	IDENTIFIER
pGL3-basic vector	Promega	Cat#E1751
pGL3-Ccl5	This paper	N/A
pGL3-Il23r	This paper	N/A
pGL3-miR-181a	This paper	N/A
pLL3.7 vector	Addgene	Cat#11795
pLL3.7-miR-181a (LV-181a)	This paper	N/A
pCDH-CMV-MCS-EF1-copGFP	System Biosciences	Cat#CD511B-1
pCDH-CMV-MCS-EF1-copGFP-Foxo3 (LV-Foxo3)	This paper	N/A
pCDH-CMV-MCS-EF1-copGFP-Myc (LV-Myc)	This paper	N/A
psPAX2 vector	Addgene	Cat#12260
pMD2.G vector	Addgene	Cat#12259
Software and algorithms		
GeneSpring GX software	Agilent Technologies	N/A
Quantity One software	Bio-Rad	https://quantity-one.software.informer.com/
FlowJo VX	Tree Star	https://flowjo-vx.software.informer.com/
SPSS 26.0 software	IBM Corporation	https://spss.en.softonic.com/
Cluster 3.0	Stanford University	https://cluster2.software.informer.com/
Integrative Genomics Viewer	Broad Institute	https://igv1.software.informer.com/
TarBase	DIANA Lab	www.microrna.gr/tarbase
Pictar	Rajewsky lab	http://pictar.mdc-berlin.de/
StarBase	Sun Yat-sen University	http://starbase.sysu.edu.cn/index.php
Targetscan	Whitehead Institute	www.targetscan.org
Other		
MACS separator system	Miltenyi Biotec	Cat#027087

RESOURCE AVAILABILITY

Lead contact

Further information and requests for resources and reagents should be directed to and will be fulfilled by the lead contact, Hong Nian (nianhong@126.com).

Materials availability

This study did not generate new unique reagents.

Data and code availability

This paper does not report original code.

miRNA microarray data were deposited in the Gene Expression Omnibus database with accession number GSE213034. Original data have been deposited at Mendeley Data Repository and are publicly available as of the date of publication. The DOI is listed in the key resources table. We downloaded the microarray profiles (GSE70403, GSE61399 and GSE145191) from the GEO database. ChIP-seq datasets were obtained from the Cistrome Project. We used the JASPAR database to predict the transcriptional factor binding sites in *Il23r*, *Ccl5*, *Il17a*, and miR-181a promoter regions. All the other data supporting the findings of this study are available within the article and its supplemental information files or available from the corresponding author upon reasonable request.

EXPERIMENTAL MODEL AND SUBJECT DETAILS

Mice

Pathogen-free female C57BL/6 mice (10 weeks old) were obtained from Vital River Laboratory Animal Technology (Beijing, China). Mice were housed in a temperature-controlled (22 ± 2°C), specific pathogen-free

barrier facility under a 12-hour light/dark cycle with a standard laboratory diet and water *ad libitum*. All animal experiments were approved by the Institutional Animal Care and Use Committee of Tianjin Medical University (ethics approval number: TJYY2019110117), in line with the requirements of the Association for Research in Vision and Ophthalmology (ARVO) Statement for the Use of Animals in Ophthalmic and Vision Research.

METHOD DETAILS

Induction of EAU and adoptive transfer

For induction of EAU by active immunization, female C57BL/6 mice (female mice were chosen as there is a higher incidence of autoimmune uveitis in women than in men (Agarwal et al., 2012; Bowers et al., 2022)) were injected intraperitoneally (i.p.) with 800 ng of pertussis toxin and immunized subcutaneously (s.c.) at over six spots on the tail base and flank with uveitogenic peptide $IRBP_{1–20}$ (200 μg per mouse) emulsified in an equal volume of complete Freund's adjuvant (CFA) containing *Mycobacterium tuberculosis* strain H37RA (0.8 mg per mouse). Interphotoreceptor retinoid-binding protein (IRBP) peptide 1–20 (aa 1–20 of human IRBP) was synthesized and purified by Sangon Biotech (Shanghai, China). *Mycobacterium tuberculosis* strain H37RA and pertussis toxin were purchased from BD Biosciences (San Jose, CA, USA) and Sigma-Aldrich, Merck (Darmstadt, Germany), respectively.

For induction of EAU by adoptive transfer, $CD4^+$ T cells from $IRBP_{1-20}$-immunized mice were transfected with Ctrl or miR-181a-5p mimics, and then transfected T cells (1×10^7 cells/well) were restimulated *in vitro* with $IRBP_{1-20}$ (10 μg/ml) in the presence of 1×10^7 irradiated (30 Gy) syngeneic splenocytes as antigen-presenting cells (APCs) under Th17 cell polarizing conditions. After 2 days, the activated T cell blasts were isolated by density gradient centrifugation (Ficoll; GE Health Care, Little Chalfont, UK) and injected i.p. into naive C57BL/6 mice (5×10^6 cells per mouse) as described previously (Nian et al., 2012; Shao et al., 2006).

Evaluation of EAU

Clinical signs of EAU were assessed by indirect fundoscopy three times a week. The pupils were dilated using 0.5% tropicamide and 1.25% phenylephrine hydrochloride ophthalmic solutions, and fundoscopic grading of the disease was performed in a blinded manner on a scale from 0 to 4 according to published scoring criteria that are based on the severity and extent of the inflammatory lesion (Agarwal et al., 2012). In brief, the clinical scoring scale is as follows: 0 = no inflammatory lesion; 0.5 = trace disease with minimal vasculitis; 1 = mildly active disease with mild vasculitis and a few small focal chorioretinal lesions; 2 = moderately active disease with severe vasculitis, multifocal chorioretinal lesions; 3 = active disease with large, confluent chorioretinal lesions, linear chorioretinal lesions, and/or hemorrhage; 4 = severely active disease with retinal detachment, hemorrhage, and/or atrophy.

For histopathological analysis, whole eyes were fixed and embedded in paraffin and sectioned in 5-μm thickness along the papillary-optic nerve axis. The sections were stained with hematoxylin and eosin (H&E). The severity of EAU was scored on a scale of 0–4, based on the cellular infiltration and structural changes, using previously reported criteria (Agarwal et al., 2012): 0 = no inflammation; 0.5 = mild cellular infiltration; 1 = moderate cellular infiltration and a few retinal folds; 2 = medium cellular infiltration, multifocal retinal folds and focal photoreceptor cell damage; 3 = heavy cellular infiltration, extensive retinal folds with detachment, serous exudates, and moderate photoreceptor cell damage; 4 = very heavy cellular infiltration, extensive photoreceptor cell damage, and retinal layer atrophy.

$CD4^+$ T cell isolation and polarization

$CD4^+$ T cells were isolated and purified from the spleen and draining lymph nodes of EAU mice by positive selection using PE-conjugated anti-mouse CD4 antibody (BioLegend, San Diego, CA, USA), anti-PE microbeads, and auto-MACS separator (Miltenyi Biotec, Bergisch Gladbach, Germany) according to the manufacturer's protocol. $CD4^+$ T cells were maintained in RPMI 1640 medium (Gibco, CA, USA) with 10% heat-inactivated fetal bovine serum (HyClone, Logan, UT, USA), 50 μM β-mercaptoethanol (Gibco), 2mM L-Glutamine (Gibco), and 100 U/mL Penicillin-Streptomycin (Gibco), referred to as complete RPMI 1640 medium. Then, $CD4^+$ T cells (1×10^6 cells/well) were co-cultured with 1×10^6 irradiated (30 Gy) syngeneic splenocytes as APCs, which were pre-incubated with 10 μg/ml $IRBP_{1-20}$ for 20 min in a 24-well plate,

under Th17 cell polarization (culture medium supplemented with 10 ng/ml IL-23) or Th1 cell polarization (culture medium supplemented with 10 ng/ml IL-12).

Transfection

siRNAs, miR-181a-5p mimics, inhibitors, and corresponding controls were synthesized by GenePharma (Shanghai, China). All sequences used are presented in Key Resources Table. miR-181a-5p mimics, inhibitors (300 nM), or siRNAs (200 nM) were transfected into $CD4^+$ T cells with Lipofectamine 2000 (Thermo Fisher Scientific, Waltham, MA, USA) following the manufacturer's instructions. Twenty-four hours after transfection, the transfected $CD4^+$ T cells were co-cultured with $IRBP_{1\text{-}20}$ (10 μg/ml) and irradiated APCs (at a ratio of 1:1) under Th17 cell polarization for additional 2 days or 8 days. Cells and supernatant were then collected for further analysis.

Real-time quantitative RT-PCR

Total RNA was extracted from the cells and tissues (including spleen, lymph nodes, thymus, and eye) with TRIzol reagent (Thermo Fisher Scientific). RevertAid First Strand cDNA Synthesis Kit (Thermo Fisher Scientific) was utilized to synthesize cDNA according to the manufacturer's protocol. Real-time quantitative RT-PCR (real-time qRT-PCR) was performed with SYBR Green Master Mix (Roche, Basel, Switzerland) on LightCycler 480 Instrument (Roche). For mRNA analysis, the gene-specific primers were used (Table S1) and values were calculated using the $2^{-\triangle\triangle Ct}$ method with glyceraldehyde-3-phosphate dehydrogenase (*Gapdh*) as an endogenous control. For miRNA analysis, the stem-loop primer method was used for the quantification of miR-181a-5p and its relative expression levels were normalized to U6 snRNA levels within each sample. The primer sequences were as follows: miR-181a-5p RT primer: 5′-CGAACATT CAACGCTGTCG-3′; miR-181a-5p Forward primer: 5′-GTCGTATCCAGTGCAGGGTCCGAGGTATTC GCACTGGATACGACACTCAC-3′; miR-181a-5p Reverse primer: 5′-AGTGCAGGGTCCGAGGTATT-3′.

Construction of plasmid

The genomic sequence spanning the mouse miR-181a-5p precursor sequence was amplified and cloned into lentiviral vector pLL3.7 (Addgene) between the Hpa I and the Xho I site. The PLL3.7 plasmid was a gift from Prof. Chunsheng Han and Dr. Jian Chen (Institute of Zoology, Chinese Academy of Science). *Rorc* coding sequence or *Myc* coding sequence was PCR amplified from mouse spleen cDNA and inserted into the Not I and EcoR I sites of pCDH-CMV-MCS-EF1-copGFP (System Biosciences), respectively. All primers used are listed in Table S2. The PCR amplification was carried out for 30 cycles using the following parameters: predenaturation at 94°C for 3 min; denaturation at 94°C for 30 sec, annealing at 67°C (*Rorc* coding sequence) or 65.5°C (*Myc* coding sequence) for 45 sec, extension at 72°C for 2 min; and a final extension step of 5 min at 72°C.

Lentivirus packaging and infection

The recombinant lentiviral plasmid was transfected into human embryonic kidney 293T cells (HEK293T) with psPAX2 (Addgene) and pMD2.G (Addgene) using Lipofectamine 2000 (Thermo Fisher Scientific). After 48 h and 72 h, the culture medium was collected and centrifuged at 2000 × g for 15 min to remove the cell debris, and then PEG8000 (Solarbio, Beijing, China) was added to concentrate the lentivirus. The titer of the lentivirus used for *in vitro* infection and *in vivo* injection was concentrated to at least 5×10^8 transducing units (TU) per milliliter. $CD4^+$ T cells were infected with lentivirus (MOI 50) by spinning at 1000 × g for 90 min in the presence of 6 μg/ml polybrene (Solarbio). Mice were given approximately 5×10^7 TU of lentivirus by tail vein injection at a volume of 200 μl/mouse. On day 7 after the systemic administration injection, mice were actively immunized with $IRBP_{1\text{-}20}$ to induce EAU. Then, the clinal and histological assessment was performed as described previously.

Intravitreal injection of miRNA

EAU mice were intravitreally injected with liposomes containing miR-181a-5p or Ctrl mimics (6 mice per group) at the onset of disease symptoms (about 11 days post-immunization). The Ctrl or miR-181a-5p mimics were complexed with liposomes to form nanoparticles for *in vivo* applications (Xiang et al., 2015). The miRNA mimics (1 mg/ml in water, 0.5 μl) were mixed with 0.5 μl lipofectamine 2000 (Thermo Fisher Scientific) for 20 min before intravitreal injection. Thereafter, 1 μl miRNA-liposome complexes were delivered into the vitreous cavity using 34-gauge Hamilton microsyringe, and the needle was kept still for 30 sec after injection to prevent leakage and reflux from the injection site.

Generation of dendritic cells

Bone marrow-derived dendritic cells (DCs) were generated by *in vitro* differentiation of bone marrow cells as previously described (Lutz et al., 1999). Briefly, bone marrow cells were flushed from femurs and tibias of mice and cultured in 12-well plate (2×10^6 cells per well) with complete RPMI 1640 medium supplemented with 10 ng/ml granulocyte-macrophage colony-stimulating factor (GM-CSF; R&D system, Minneapolis, MN, USA) and 10 ng/ml interleukin-4 (IL-4; R&D system). On day 6, non-adherent cells were harvested for phenotyping and further experiments.

For DCs transfection, DCs were transfected with miR-181a-5p or Ctrl mimics in 24-well plate (2.5×10^5 cells per well) using Lipofectamine 2000 (Thermo Fisher Scientific). At 24 h after transfection, DCs were treated with 100 ng/mL of lipopolysaccharide (LPS) and subjected to real-time qRT-PCR analysis.

For co-cultured study, the transfected DCs were pre-incubated with $IRBP_{1\text{-}20}$ (10 μg/ml) for 20 min, and then co-cultured with $CD4^+$ T cells at a ratio of 1:10 under Th17 cell polarization for 2 days or 8 days. Then the cells were collected for real-time qRT-PCR or flow cytometry analysis.

Flow cytometry

For surface staining, cells were incubated with Fc-block (BioLegend) and stained with the following antibodies from BioLegend: PE-conjugated anti-mouse CD4 antibody (clone GK1.5), or FITC-conjugated anti-mouse CD4 antibody (clone H129.19). For intracellular staining, cells were stimulated for 4-6 h at 37°C in complete RPMI 1640 medium with phorbol myristate acetate (50 ng/ml), ionomycin (1 μg/ml), and brefeldin A (1 μg/ml) (Sigma-Aldrich, Merck), followed by fixation and permeabilization using Fixation and Permeabilization kit (eBioscience, SanDiego, CA, USA). FITC-conjugated anti-mouse IL-17 antibody (clone TC11-18H10.1) and PE-conjugated anti-mouse Foxp3 antibody (clone FJK-16s) were used for intracellular staining. Stained cells were analyzed with a FACSCalibur flow cytometer (BD Biosciences). FlowJo software (Tree star, Ashland, OR, USA) was used to analyze the acquired data.

Enzyme-linked immunosorbent assay (Elisa)

The cytokines in the culture supernatants were detected with Mouse IL-17 DuoSet ELISA Kit (R&D Systems, Minneapolis, MN, USA) and Mouse IFN-gamma DuoSet ELISA Kit (R&D Systems) according to the manufacturer's instructions. Briefly, 96-well plates were coated with the capture antibodies overnight at room temperature. After washing and blocking, the diluted supernatants and recombinant cytokine standards were added to the plates and incubated for 2 h at room temperature. Then, the plates were incubated sequentially with the detection antibodies and streptavidin-HRP, as well as Substrate Reagent (R&D Systems) and Stop Solution. The absorbance was measured at 450 nm with wavelength correction set to 540 nm.

miRNA microarray

RNA samples were extracted from $CD4^+$ T cells of naïve or EAU mice using TRIzol reagent (Thermo Fisher Scientific) and subjected to miRNA array analysis by 8 × 60 K miR Microarray (Agilent Technologies, Santa Clara, CA, USA). The microarray was performed by CapitalBio Corporation (Beijing, China), and microarray data were analyzed using the GeneSpring GX software (Agilent Technologies).

Luciferase assay

Firstly, the wild-type (WT) *Akt3* 3′ UTR fragment containing the putative miR-181a-5p binding site or mutant (mut) *Akt3* 3′ UTR fragment was amplified and cloned into pMIR-REPORT Vector (Promega, Madison, WI, USA) between the Hind III and Spe I site as we described previously (Wei et al., 2019). For PGL3 plasmids harboring *Il23r* promoter, *Ccl5* promoter, or miR-181a promoter, the promoter regions were amplified and cloned into pGL3-basic (Promega) between the Kpn I and Xho I site. All primers used are listed in Table S2. HEK293T cells (2.5×10^4 cells/well) or EL4 T cells (3×10^4 cells/well) were seeded in 96-well plates, and co-transfected with indicated oligonucleotides and plasmids using Lipofectamine 2000 (Thermo Fisher Scientific), and PRL-TK vector (Promega, Madison, WI, USA) was used as the internal control. Forty-eight hours after transfection, cell extracts were prepared using passive lysis buffer (Promega), and luciferase activity was detected by the Dual-Luciferase Assay System (Promega) following the manufacturer's instructions. Firefly luciferase activity was normalized with Renilla luciferase activity.

Western blot analysis

Proteins were extracted from $CD4^+$ T cells using RIPA lysis buffer (Solarbio, Beijing, China) accompanied by protease inhibitor PMSF (Solarbio) and phosphatase inhibitor cocktail (Cell Signaling Technology), and concentrations were determined with a BCA protein assay kit (Solarbio). 30 μg of protein were electrophoresed by SDS-PAGE and transferred onto PVDF membranes. The membranes were blocked with 5% non-fat milk for 2 h and incubated with the antibodies specific for AKT3, Phospho-AKT (Ser473), Phospho-FOXO3 (Thr32) (Cell Signaling Technology, Danvers, MA, USA) or β-actin (Santa Cruz Biotechnology, Dallas, TX, USA) at 4°C overnight. HRP-conjugated secondary antibody (ZSGB-BIO, Beijing, China) was applied at room temperature for 2 h. Signals were visualized using ECL reagent, and the optical density of the protein bands was quantified by Quantity One software (Bio-Rad, Hercules, CA, USA).

Immunofluorescence staining

LV-181a- or LV-Ctrl-infected EL4 T cells were fixed with 4% paraformaldehyde (Solarbio) at room temperature for 15 min and then permeabilized with 0.3% TritonX-100 (Solarbio) for 10 min. After blocking with 5% goat serum (Solarbio) for 1 h, EL4 T cells were incubated with rabbit anti-FOXO3 (Cell Signaling Technology) primary antibody overnight at 4°C. The following day, the cells were incubated with the goat anti-rabbit Alexa Fluor® 594 (IgG H&L) (Abcam, Cambridge, MA, USA) at room temperature for 1 h and subsequently the nuclei were counterstained with DAPI (Sigma-Aldrich, Merck). Fluorescence images were obtained using a confocal fluorescence microscope (LSM800, Zeiss, Oberkochen, Germany) with a ×63 oil immersion objective.

Bioinformatics analysis

Potential target genes of miR-181a-5p were predicted by TarBase (www.microrna.gr/tarbase), Pictar (https://pictar.mdc-berlin.de/), StarBase (http://starbase.sysu.edu.cn) and Targetscan (www.targetscan.org) databases. The predicted target genes are listed in Table S3.

The microarray profiles (GSE70403, GSE61399, and GSE145191) were obtained from the Gene Expression Omnibus (GEO) database (http://www.ncbi.nlm.nih.gov/geo/). Heatmaps were generated with Cluster 3.0 software (Stanford University). ChIP-seq datasets were obtained from the Cistrome Project (http://www.cistrome.org/). ChIP-seq genomic tracks were visualized using Integrative Genomics Viewer (IGV) tool.

QUANTIFICATION AND STATISTICAL ANALYSIS

SPSS 26.0 software (IBM Corporation, Somers, NY, USA) was used for statistical analysis. All experiments were repeated 3 times or more, and the data were presented as mean ± SEM. The normal distribution of the data was evaluated by Shapiro-Wilk test. According to the normality of data and the number of groups, Student's t-test, Mann-Whitney U test, the Kruskal-Wallis test, One-way ANOVA or two-way ANOVA were then selected respectively. Correlation analysis was evaluated by the Pearson correlation test. P values of less than 0.05 were considered statistically significant.